

Distribution Matching in Variational Inference

Mihaela Rosca¹ Balaji Lakshminarayanan¹ Shakir Mohamed¹

Abstract

The difficulties in matching the latent posterior to the prior, balancing powerful posteriors with computational efficiency, and the reduced flexibility of data likelihoods are the biggest challenges in the advancement of Variational Autoencoders. We show that these issues arise due to struggles in marginal divergence minimization, and explore an alternative to using conditional distributions that is inspired by Generative Adversarial Networks. The class probability estimation that GANs offer for marginal divergence minimization uncovers a family of VAE-GAN hybrids, which offer the promise of addressing these major challenges in variational inference. We systematically explore the solutions available for distribution matching, but show that these hybrid methods do not fulfill this promise, and the trade-off between generation and inference that they give rise to remains an ongoing research topic.

1. Introduction

This paper focuses on the challenges of training variational auto-encoders (Kingma and Welling, 2013; Rezende et al., 2014): the struggles of matching the marginal latent posterior distribution with the latent prior; the limitations of simple Gaussian diagonal latent posteriors, and the lack of likelihoods that capture the semantic similarity of data (like perceptual similarity in images). We show that all these issues can be tackled by matching *marginal* distributions instead of *conditional* distributions. A common approach to matching marginal distributions was popularized by generative adversarial networks (Goodfellow et al., 2014) and leverages the power of classifiers for density ratio estimation and divergence minimization. This can be done in latent space, data space, or joint space and leads to different model variants that trade-off by the uncertainty estimation provided the evidence lower bound for the promise of a more powerful tool to match distributions.

Variational auto-encoders (VAEs) and generative adversarial

¹DeepMind. Correspondence to: Mihaela Rosca <mihaelacr@google.com>.

networks (GANs) are popular latent variable algorithms used for learning in latent variable models that are used for data generation and inference. Data generation allows for applications in semi-supervised learning (Kingma et al., 2014; Salimans et al., 2017), in-painting (Nguyen et al., 2016), image-to-image translation (Kim et al., 2017; Zhu et al., 2017), while posterior inference is used in a broad range of applications in representation learning in different domain applications such as reinforcement learning, few-shot learning and counterfactual reasoning (Higgins et al., 2017b; Louizos et al., 2017; Mathieu et al., 2016; Rezende et al., 2016; van den Oord et al., 2017). As we continue to scale these models and deploy them in wider applications, it is vital that we develop a deeper understanding of their shortcomings. This is the aim of this paper, and in doing so we make the following contributions:

- With an extensive analysis, and over varying dimensionality, we expose a core issue of variational inference: the difficulty of matching the marginal latent posterior to the prior distribution.
- Classifiers offer the hope of an alternative methods for computing KL divergences. But we show that they are poor estimators of the *value* of the divergence. Despite this, we demonstrate that classifiers are effective tools when used for *learning*, but also show that they do not scale to high dimensions.
- VAE-GAN hybrids aim to improve on both VAEs and GANs, by incorporating adversarial training for distribution matching. These hybrid approaches are often developed with the aim of providing increased stability and performance. Using a battery of tests, we compare these hybrids to VAEs, DRAW and GANs to expose their advantages and shortcomings: they allow for posterior inference in implicit generative models; they only perform on par with GANs but not better; and they lose the property of maintaining a likelihood bound that can be used for model evaluation and comparison.

2. Challenges in Variational Inference

Latent variable models use an unobserved latent variable \mathbf{z} to build a model of the visible data distribution $p^*(\mathbf{x})$ either by defining a conditional probability distribution $p_{\theta}(\mathbf{x}|\mathbf{z})$ or learning a direct, deterministic, mapping $G : \mathbf{z} \rightarrow \mathbf{x}$. These models are particularly suitable for data that lies on a lower

dimensional manifold - as is the case for natural images, music and text. Latent variables are desirable since they can be used to capture the underlying structure of the data, or leverage our knowledge of the data generating process. This underlying structure can be used in applications such as discovering topics in text (Blei et al., 2003) or for dimensionality reduction, denoising and visualization (Smith, 2002).

A popular approach for learning latent variable models is variational inference. Variational inference is driven by the computation of marginal likelihood:

$$p_{\theta}(\mathbf{x}) = \int p_{\theta}(\mathbf{x}|\mathbf{z})p(\mathbf{z})d\mathbf{z} \quad (1)$$

As the integral in equation 1 is intractable, a variational distribution $q_{\eta}(\mathbf{z}|\mathbf{x})$ is introduced via the variational lower bound of $p_{\theta}(\mathbf{x})$:

$$\log p_{\theta}(\mathbf{x}) \geq \underbrace{\mathbb{E}_{q_{\eta}(\mathbf{z}|\mathbf{x})}[\log p_{\theta}(\mathbf{x}|\mathbf{z})]}_{\text{likelihood term}} - \underbrace{\text{KL}[q_{\eta}(\mathbf{z}|\mathbf{x})||p(\mathbf{z})]}_{\text{KL term}} \quad (2)$$

The bound holds for any distribution $q_{\eta}(\mathbf{z}|\mathbf{x})$, but by optimizing the parameters η , the bound can be made tighter. The training objective then becomes to learn the parameters θ of the model used to represent $p_{\theta}(\mathbf{x}|\mathbf{z})$, the decoder, and the parameters η of the distribution $q_{\eta}(\mathbf{z}|\mathbf{x})$, the encoder, to maximize the evidence lower bound (ELBO):

$$\mathbb{E}_{p^*(\mathbf{x})} [\mathbb{E}_{q_{\eta}(\mathbf{z}|\mathbf{x})}[\log p_{\theta}(\mathbf{x}|\mathbf{z})] - \text{KL}[q_{\eta}(\mathbf{z}|\mathbf{x})||p(\mathbf{z})]] \quad (3)$$

The competition between these two terms introduces an inference-generation trade-off:

- The likelihood term $\mathbb{E}_{q_{\eta}(\mathbf{z}|\mathbf{x})}[\log p_{\theta}(\mathbf{x}|\mathbf{z})]$ ensures that $q_{\eta}(\mathbf{z}|\mathbf{x})$ encodes enough information about \mathbf{x} such that it has high likelihood under the reconstruction distribution $p_{\theta}(\mathbf{x}|\mathbf{z})$, $z \sim q_{\eta}(\mathbf{z}|\mathbf{x})$.
- The term $\text{KL}[q_{\eta}(\mathbf{z}|\mathbf{x})||p(\mathbf{z})]$ matches the posterior $q_{\eta}(\mathbf{z}|\mathbf{x})$ to the prior $p(\mathbf{z})$ which does not encode any information about \mathbf{x} , thus encouraging encoding less information about \mathbf{x} in the posterior.

We can do a "surgery on the ELBO" (Hoffman and Johnson, 2016) to reveal this in another way:

$$\mathbb{E}_{p^*(\mathbf{x})} \text{KL}[q_{\eta}(\mathbf{z}|\mathbf{x})||p(\mathbf{z})] \quad (4)$$

$$= \text{KL}[q_{\eta}(\mathbf{z})||p(\mathbf{z})] + \mathbb{I}[q_{\eta}(\mathbf{z}|\mathbf{x})p^*(\mathbf{x})] \quad (5)$$

$$\text{where } q_{\eta}(\mathbf{z}) = \int q_{\eta}(\mathbf{z}|\mathbf{x})p^*(\mathbf{x})d\mathbf{x} \quad (6)$$

is the marginal (a.k.a. aggregate) posterior over latents and \mathbb{I} denotes mutual information. Because the mutual information between two distribution is non-negative, minimizing $\mathbb{E}_{p^*(\mathbf{x})} \text{KL}[q_{\eta}(\mathbf{z}|\mathbf{x})||p(\mathbf{z})]$ minimizes an upper

bound on $\text{KL}[q_{\eta}(\mathbf{z})||p(\mathbf{z})]$. By bringing $q_{\eta}(\mathbf{z})$ closer to $p(\mathbf{z})$, the model distribution $p_{\theta}(\mathbf{x}) = \int p_{\theta}(\mathbf{x}|\mathbf{z})p(\mathbf{z})d\mathbf{z}$ is brought close to the marginal reconstruction distribution $\int p_{\theta}(\mathbf{x}|\mathbf{z})q_{\eta}(\mathbf{z})d\mathbf{z}$. Variational inference models learn to sample by maximizing reconstruction quality - via the likelihood term - and reducing the gap between samples and reconstructions - via the KL term. Failure to match $q_{\eta}(\mathbf{z})$ and $p(\mathbf{z})$ results in regions in latent space that have high mass under $p(\mathbf{z})$ but not under $q_{\eta}(\mathbf{z})$. This means that prior samples $z \sim p(\mathbf{z})$, passed through the decoder to obtain a model sample, are likely to be far in latent space from inputs the decoder saw during training. It is this distribution mismatch that results in poor generalization performance from the decoder, and hence bad model samples.

Equation 5 shows that minimizing the conditional divergence as done in variational inference is advantageous as it does not require knowledge of $q_{\eta}(\mathbf{z})$, which is computationally expensive to approximate, while by carefully choosing the distribution family of $q_{\eta}(\mathbf{z}|\mathbf{x})$ and $p(\mathbf{z})$, $\text{KL}[q_{\eta}(\mathbf{z}|\mathbf{x})||p(\mathbf{z})]$ can be computed analytically or approximated cheaply, eg. with normalizing flows (Kingma et al., 2016; Rezende and Mohamed, 2015). The downside is that minimizing conditional divergences is an inefficient way to minimize marginal divergences - as opposed to devising a cost function which directly matches the marginals.

Throughout this paper, we will explore the ramifications of conditional distribution matching on VAEs (Kingma and Welling, 2013; Rezende et al., 2014), a model that combines variational inference with the power of neural networks as function approximators by representing $q_{\eta}(\mathbf{z}|\mathbf{x})$ and $p_{\theta}(\mathbf{x}|\mathbf{z})$ using neural networks. The encoder and decoder parameters are trained jointly using stochastic gradient descent, via the reparameterization trick (Fu, 2006; Kingma and Welling, 2013; Rezende et al., 2014).

3. Distribution matching using density ratios

The alternative to the conditional matching approach is to directly match marginal distributions. We will not have access to the marginal density, so instead we leverage the ability of classifiers to estimate density ratios, via the density ratio trick (Goodfellow et al., 2014; Goodfellow, 2014; Sugiyama et al., 2012). Under the assumption that can we train a perfect binary classifier \mathcal{D} to associate the label $y = 1$ to samples from $p_1(\mathbf{x})$ and the label $y = 0$ to samples from $p_0(\mathbf{x})$, the following holds:

$$\frac{p_1(\mathbf{x})}{p_0(\mathbf{x})} = \frac{p(y=1|\mathbf{x})}{p(y=0|\mathbf{x})} = \frac{\mathcal{D}}{1-\mathcal{D}} \quad (7)$$

We exploit class probabilities for density ratio estimation, as well as for learning, by replacing density ratios in cost functions to match marginal distributions in latent and data space.

GANs (Goodfellow et al., 2014) use the density ratio trick to match the data distribution $p^*(\mathbf{x})$ with the marginal model distribution $p_\theta(\mathbf{x})$. GANs make use of *implicit latent variable models* (Mohamed and Lakshminarayanan, 2016) and do not require observation likelihoods - they define $p_\theta(\mathbf{x})$ by specifying a deterministic mapping $G : \mathbf{z} \rightarrow \mathbf{x}$ via an adversarial game, where the generator produces samples by applying G to samples from $p(\mathbf{z})$. Unlike variational inference models, GANs do not do conditional distribution matching and have a training cost to ensure model sample quality, thus avoiding the inference-generation trade-off. They learn by using a discriminator to distinguish between generated samples and real data samples given by the dataset. In the original GAN formulation, the training was given by the min-max bi-level optimization with value function:

$$\max_D \min_G \mathbb{E}_{p^*(\mathbf{x})} [\log D(\mathbf{x})] + \mathbb{E}_{p(\mathbf{z})} [\log(1 - D(G(\mathbf{z})))]$$

Instead of using the generator loss that results from treating the game as a min-max zero sum game, an alternative non-saturating generator loss $\mathbb{E}_{p_\theta(\mathbf{x})} [-\log \mathcal{D}_\phi(\mathbf{x})]$ is used in practice, as it provides better gradients when the discriminator is confident that the generated samples are fake. Many GAN variants that use different losses have been introduced (Arjovsky et al., 2017; Mao et al., 2016; Mohamed and Lakshminarayanan, 2016; Nowozin et al., 2016; Zhao et al., 2017), but the adversarial game remains the same.

4. Inference-Generation trade-off in VAEs

4.1. ELBO Surgery in large datasets

Hoffman and Johnson (2016) use Monte Carlo estimation to show that VAEs with a small number of latents trained on binary MNIST are unable to match the $q_\eta(\mathbf{z})$ and $p(\mathbf{z})$. To the best of our knowledge, no extensive study has been previously performed showing the prevalence of this issue across data sets, large latent sizes, models and approaches of approximating $\text{KL}[q_\eta(\mathbf{z})||p(\mathbf{z})]$.

We approximate $\text{KL}[q_\eta(\mathbf{z})||p(\mathbf{z})] = \mathbb{E}_{q_\eta(\mathbf{z})} \left[\log \frac{q_\eta(\mathbf{z})}{p(\mathbf{z})} \right]$ using three methods: a Monte Carlo approach that estimates $q_\eta(\mathbf{z})$ by $\frac{1}{N} \sum_{n=1}^N q(\mathbf{z}|x_n)$; using the density ratio approach by learning class probabilities to estimate $\frac{q_\eta(\mathbf{z})}{p(\mathbf{z})}$, and a direct approach of learning $q(\mathbf{z})$ using a parametric density model. Pseudocode for these approaches can be found in Appendix A.

We trained VAEs with diagonal Gaussian posteriors on ColorMNIST (Metz et al., 2017), CelebA (Liu et al., 2015) at 64 image resolution and CIFAR-10 (Krizhevsky, 2009) and show that the issue is consistent across datasets and latent sizes and contrast the results with models with powerful

Table 1. Estimating marginal KLs via Monte Carlo estimation (MCE) for VAEs. All KL values are in nats/dim. Standard VAEs were trained using a Gaussian latent posterior and a Bernoulli distribution for $p_\theta(\mathbf{x}|\mathbf{z})$. DRAW (Gregor et al., 2015) was trained as described in Gregor et al. (2016). We used the entire training and validation sets to estimate $q_\eta(\mathbf{z})$ and the average KL term

$$\frac{1}{N} \sum_{n=1}^N \text{KL}[q_\eta(\mathbf{z}|x_n)||p(\mathbf{z})], \text{ which is computed analytically.}$$

| Model | Dataset | Number latents | Avg. KL term | MCE of $\text{KL}[q_\eta(\mathbf{z}) p(\mathbf{z})]$ |
|-------|-------------|----------------|--------------|---|
| VAE | Color MNIST | 50 | 0.468 | 0.244 |
| VAE | Color MNIST | 100 | 0.238 | 0.129 |
| VAE | CelebA | 100 | 1.1237 | 1.0039 |
| VAE | CelebA | 200 | 0.575 | 0.5138 |
| VAE | CIFAR10 | 100 | 0.447 | 0.334 |
| VAE | CIFAR10 | 200 | 0.221 | 0.164 |
| DRAW | CIFAR10 | 49152 | 0.0872 | 0.0870 |

auto-regressive posteriors.

Our results are summarized in Table 1 and Figure 1. Across all experiments, we consistently see:

- VAEs with diagonal Gaussian posteriors are not able to match the marginal $q_\eta(\mathbf{z})$ with the prior $p(\mathbf{z})$. This is in line with Hoffman and Johnson (2016) and shows that the likelihood term dominates in the evidence lower bound (equation 2) and explains why often VAEs produce good reconstructions, but poor samples.
- Models with powerful auto-regressive variational posteriors such as DRAW are able to overcome the limitations of traditional VAEs.
- Using the density ratio trick to estimate $\frac{q_\eta(\mathbf{z})}{p(\mathbf{z})}$ directly results in an underestimated value of the marginal KL. This is consistent across architectural choices for the classifier.
- Estimating $q_\eta(\mathbf{z})$ by direct density estimation results in an underestimated value of the marginal KL and suggests that $q_\eta(\mathbf{z})$ is a complex distribution, making it hard to learn it using a density estimator. This is also shows the failure of the KL term to match $q_\eta(\mathbf{z})$ to the prior, since the prior $p(\mathbf{z})$ is an isotropic Gaussian, which should be easy to learn. This is consistent across the density models we used; Masked Auto-regressive Flows (Papamakarios et al., 2017), Gaussian Mixture Model, and a Gaussian auto-regressive models learned using an LSTM (Hochreiter and Schmidhuber, 1997).

Experimental details can be found in Appendix A and all hyperparameters are given in Appendix K.

4.2. The effect of the pixel distribution choice

Balancing inference and generation in VAEs is not only a result of posterior latent distributions, or encoder and decoder choice. The distribution used to model $p_\theta(\mathbf{x}|\mathbf{z})$ also has a strong effect.

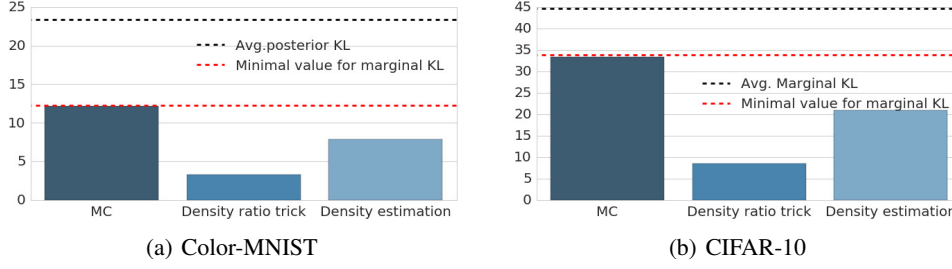


Figure 1. Estimating $\text{KL}[q_\eta(\mathbf{z})||p(\mathbf{z})]$ for standard VAEs, using Monte Carlo approximation, the density ratio trick to estimate $\frac{q_\eta(\mathbf{z})}{p(\mathbf{z})}$ and a density model to estimate $q(\mathbf{z})$. The average marginal KL is computed analytically from the trained model. The minimal value for the marginal KL (computed from equation 5) is a theoretical bound, since the mutual information term is bounded above by $\log N$, where N is the size of the training set. Density estimation values reported here are obtained using a Gaussian auto-regressive model learned using an LSTM, since it was the best performing density model.

We trained the same VAE architecture using Bernoulli and Quantized Normal visible distributions. A Quantized Normal distribution is a normal distribution with uniform noise $\mathbf{u} \in [0, 1]$ added to discrete pixel data, see Theis et al. (2016). There is a stark contrast between the results obtained using the two distributions: a Bernoulli distribution is more effective at generation, while a Quantized Normal is more effective at inference. The gradients obtained from a Bernoulli distribution have the same effect as using a Quantized Normal using variance 1, so the Bernoulli distribution cannot capture data subtleties as well as the Quantized Normal can. Since reconstructions do not encode all the details in the input, the latent posterior is less specialized, which results in a smaller KL term and better samples. The opposite occurs for a Quantized Normal: the reconstructions are very good, but the model ignores the KL term, forming a big gap between samples and reconstructions. Samples and reconstructions are shown in Appendix D, together with a formal justification.

5. Learning with density ratios

Although density ratio estimation cannot be used to estimate the KL divergence, it can be used for learning. We show that by devising a set of synthetic experiments where the true KL divergence is known and where we can determine how this approach scales with data dimensionality.

We use Gaussian distributions, defined by passing a random normal vector through an affine transformation with $W \in \mathbb{R}^{kd}$, $b \in \mathbb{R}^d$, $z \in \mathbb{R}^k$:

$$z \sim \mathcal{N}(0, \mathbb{I}_k), x = W^\top z + b \implies x \sim \mathcal{N}(b, W^\top W) \quad (8)$$

To ensure $W^\top W$ is full rank, we set $d = k/10$ in all our experiments.

We first train a classifier to distinguish between two such Gaussian distributions, for varying values of d . In the first setting, we are concerned with *divergence estimation*, keep-

ing both distributions fixed and only learn the density ratio using the classifier. Once the classifier is trained, we report the difference between the estimated and true KL divergence values. In the second setting, we are concerned with *divergence minimization* and we begin with the same initialization for the two distributions, but learn the parameters of the second Gaussian (W and b in equation 8) to minimize the estimated divergence between the two distributions. This is a GAN training regime, where the generator loss is given by the reverse KL generator loss (Mohamed and Lakshminarayanan, 2016): $-\log \frac{D(\mathbf{x})}{1-D(\mathbf{x})}$. We track the true KL divergence during training together with the online classifier estimated divergence - we should not expect the latter to be accurate, the classifier is not trained to optimality for each update of the learned distribution, as the two models are trained jointly.

If for the same classifier that failed to approximate the true KL divergence in the estimation experiments we observe a decrease in true divergence in the learning experiments, we can conclude that while the density ratio trick might not be a useful for estimation, it can still be used as an optimization tool. To ensure our conclusions are valid, we control over hyper-parameters, classifier architectures and random seeds of the Gaussian distributions, and average results over 10 runs.

Our main findings are summarized in Figure 2 and reveal that using density ratios for learning does not reliably scale with data dimensionality. For lower dimensional data (1 and 10 dimensions), the model is able to decrease the true KL divergence. However, for higher dimensional Gaussians (dimensions 100 and 1000), a classifier with 100 million parameters (4 layer MLP) is not able to provide useful gradients and learning diverges (rightmost plot in Figure 2). Regardless of data dimensionality, the estimate of the true KL divergence provided by the density ratio trick was not accurate. Details and additional experiments are specified

in the Appendix E.

6. Adversarial and Variational hybrids

The density ratio trick is a potential solution for the main challenges of VAEs: using implicit encoders and decoders (Huszár, 2017) can solve the lack of flexibility with the variational posterior and observation likelihoods and could fix the divergence minimization issues by directly matching marginal distribution, instead of conditional distributions. However, given the complications that come with using the density ratio trick, replacing terms in the variational lower bound with density ratios comes with its own difficulties. As we showed in Section 5, class probabilities from discriminators can be used for divergence minimization, but the provided ratio is not accurate, and thus cannot be used to estimate the evidence lower bound of the test data log likelihood, which is reported as a quality measure when training VAEs. So while all VAE-GAN variants do posterior inference, they are affected by this issue and lack a standard inference metric (plots in the Appendix, Section F). In this section we further explore the benefits and challenges of VAE-GAN hybrids.

The models discussed below are visualized in Figure 3.

6.1. Replacing $\mathbb{KL}[q_\eta(\mathbf{z}|x_n)||p(\mathbf{z})]$

The VAE approach to matching $q_\eta(\mathbf{z})$ and $p(\mathbf{z})$ by introducing $\mathbb{E}_{p^*(\mathbf{x})} [\mathbb{KL}[q_\eta(\mathbf{z}|x_n)||p(\mathbf{z})]]$ as an upper bound to $\mathbb{KL}[q_\eta(\mathbf{z})||p(\mathbf{z})]$ does not only introduce the inference-generation trade-off, but also limits the family of distributions that can be used to model $q_\eta(\mathbf{z}|\mathbf{x})$: $\log q_\eta(\mathbf{z}|\mathbf{x})$ has to be easy to compute. The density ratio trick provides an alternative which avoids any restrictions on $q_\eta(\mathbf{z}|\mathbf{x})$, since it does not require computing $\log q_\eta(\mathbf{z}|\mathbf{x})$ to estimate $\mathbb{KL}[q_\eta(\mathbf{z}|x_n)||p(\mathbf{z})]$, but only samples from the distribution. However, directly replacing the divergences in equation 3 with a density ratio is challenging, as we need to estimate a KL term for each datapoint, making it both memory intensive and hard to train due to limited data for each discriminator.

AdversarialVB (Mescheder et al., 2017) circumvents this issue by training a discriminator which estimates all ratios by having access to \mathbf{x} : it learns to distinguish between pairs $(x \sim p^*(\mathbf{x}), z \sim p(\mathbf{z}))$ and $(x \sim p^*(\mathbf{x}), z \sim q_\eta(\mathbf{z}|\mathbf{x}))$. While theoretically sound - under infinite data and perfect optimization the discriminator learns to estimate $\frac{q(\mathbf{z}|\mathbf{x})}{p(\mathbf{z})}$ for $x \sim p^*(\mathbf{x})$ - AdversarialVB has issues in practice as it is hard for the parametric discriminator to learn to ignore \mathbf{x} when classifying $(x \sim p^*(\mathbf{x}), z \sim p(\mathbf{z}))$. To overcome, this the authors propose adaptive contrast (Mescheder et al., 2017), which introduces an auxiliary density to help estimating the KL. In our experiments without adaptive contrast it

severely underperformed other models (see Appendix J).

Adversarial auto-encoders (AAE) (Makhzani et al., 2015) avoid estimating $\mathbb{E}_{p^*(\mathbf{x})} [\mathbb{KL}[q_\eta(\mathbf{z}|x_n)||p(\mathbf{z})]]$ altogether, and use a discriminator to learn $\mathbb{KL}[q_\eta(\mathbf{z})||p(\mathbf{z})]$ and provide gradients to match $q_\eta(\mathbf{z})$ and $p(\mathbf{z})$. By not having a cost on the conditional $q_\eta(\mathbf{z}|\mathbf{x})$ matching the prior, AAE can use any posterior latent distribution, and can avoid the inference-generation trade-off, as long as the discriminator ensures the marginal matches the prior. Wasserstein auto-encoders (Tolstikhin et al., 2018) extend AAE to minimize Wasserstein distance between the marginal posterior and the prior over latent variables.

6.2. The likelihood term

We have discussed how two limitations of VAEs - the assumptions regarding the posterior latent distribution $q_\eta(\mathbf{z}|\mathbf{x})$ and the difficulty of matching $q_\eta(\mathbf{z})$ and $p(\mathbf{z})$ - can be tackled using the density ratio trick. We now turn our attention to a third issue: observation likelihoods. Problems with observation likelihoods are notorious: assuming a Gaussian or Laplacian likelihood results in blurry samples and reconstructions. Given that GANs do not have this issue, it is tempting to use the density ratio trick in the likelihood term. The approach of replacing the likelihood term in the variational lower bound (2) with a substitute is a form of synthetic likelihood (Dutta et al., 2016; Wood, 2010).

A ratio can be introduced in the likelihood term of (2) by dividing and multiplying by the true data distribution $p^*(\mathbf{x})$:

$$\begin{aligned} \mathbb{E}_{q_\eta(\mathbf{z}|\mathbf{x})} [\log p_\theta(\mathbf{x}|\mathbf{z})] = \\ \mathbb{E}_{q_\eta(\mathbf{z}|\mathbf{x})} \left[\log \frac{p_\theta(\mathbf{x}|\mathbf{z})}{p^*(\mathbf{x})} \right] + \mathbb{E}_{q_\eta(\mathbf{z}|\mathbf{x})} [\log p^*(\mathbf{x})] \quad (9) \end{aligned}$$

The second term in (9) is independent of θ and can be ignored for optimization purposes. We would like to use the density ratio trick to estimate the first term in (9) but face two problems:

1. Naively using the density ratio trick requires an infinite number of discriminators: we need to train one discriminator for each $p_\theta(\mathbf{x}|\mathbf{z})$ with $z \sim q(\mathbf{z}|x_n)$. We could use the AdversarialVB approach, and train a joint discriminator to approximate all ratios, but as we have seen, this approach has downsides in practice.
2. Replacing the ratio in equation 9 with a discriminator \mathcal{D} which approximates $\frac{p_\theta(\mathbf{x}|\mathbf{z})}{p^*(\mathbf{x})}$ results in no gradients for the decoder. Since the expectation in the loss is taken w.r.t. *data distribution*, the new optimization objective is: $\mathbb{E}_{p^*(\mathbf{x})} \mathbb{E}_{q_\eta(\mathbf{z}|\mathbf{x}_n)} \log \mathcal{D}(\mathbf{x}, \mathbf{z})$. The new objective no longer has an expectation w.r.t. to the decoder parameters θ , which was made explicit in the observed likelihood case - the model samples are now only used to train \mathcal{D} .

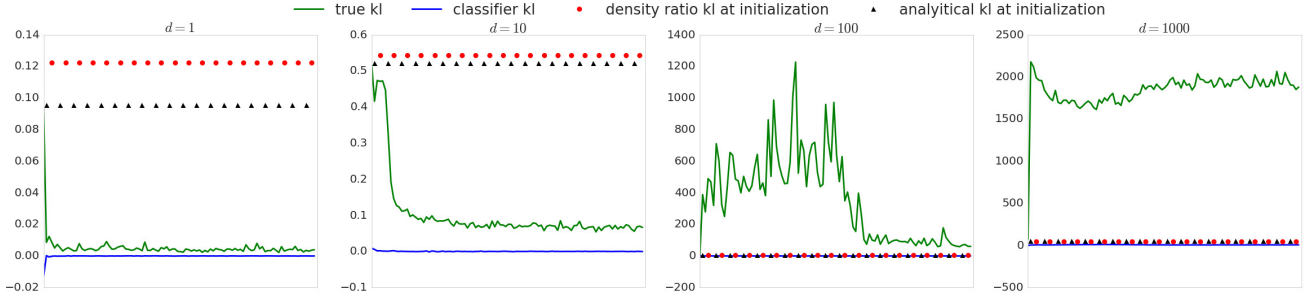


Figure 2. Divergence estimation and minimization of Gaussian distributions, for different data dimensions d . We plot training progress using the true KL divergence between the learned and true distributions. As a reference point, we plot the true KL divergence at initialization, together with how well the same classifier architecture is able to estimate the initial true KL when the two Gaussian distributions are stationary. Results are averaged over 10 different initializations for the classifier.

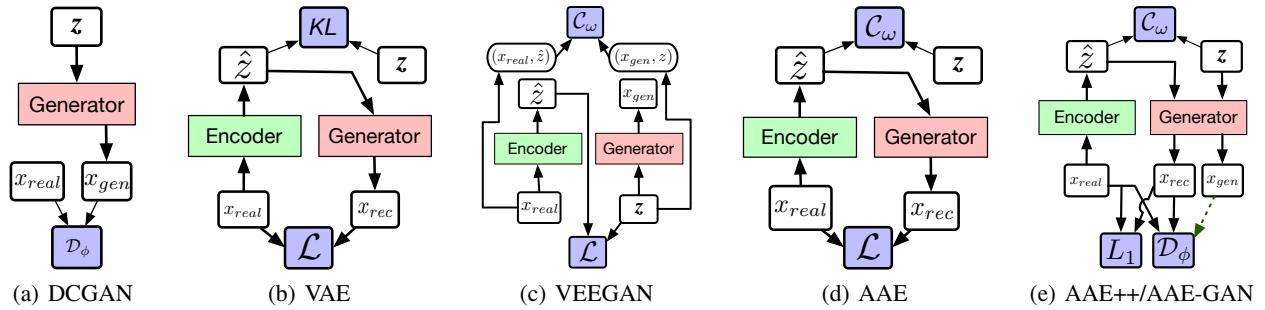


Figure 3. Architectures for models used in our comparisons. (WGAN is similar to DCGAN.) The difference between AAE-GAN and AAE++ is given by the cost on model samples exemplified using the green arrow between x_{gen} and \mathcal{D}_ϕ .

Hence applying the density ratio trick to the likelihood term is not straight forward. These limitations can be overcome by a different approach, introduced by VEEGAN (Srivastava et al., 2017). VEEGAN uses a reconstructor network to learn a posterior distribution $p_\gamma(\mathbf{z}|\mathbf{x})$. Unlike in standard variational inference, the VEEGAN objective is to minimize the cross entropy between the marginal latent distribution induced by the reconstructor $p_\gamma(\mathbf{z}) = \int p_\gamma(\mathbf{z}|\mathbf{x})p^*(\mathbf{x})$ and the prior $p(\mathbf{z})$. Because $p_\gamma(\mathbf{z})$ is intractable, $p_\theta(\mathbf{x}|\mathbf{z})$ is introduced as a variational distribution using the lower bound $\int p_\gamma(\mathbf{z}|\mathbf{x})p^*(\mathbf{x})d\mathbf{x} \leq \text{KL}[p_\theta(\mathbf{x}|\mathbf{z})p(\mathbf{z})||p_\gamma(\mathbf{z}|\mathbf{x})p^*(\mathbf{x})] + C$, where C is a constant. The model is trained to minimize the negative of the lower bound and a reconstruction loss in latent space. To estimate $\text{KL}[p_\theta(\mathbf{x}|\mathbf{z})p(\mathbf{z})||p_\gamma(\mathbf{z}|\mathbf{x})p^*(\mathbf{x})]$, VEEGAN uses the density ratio trick on joint distributions. Since the expectation in the objective is not taken with respect to the data distribution $p^*(\mathbf{x})$ but the joint distribution $p_\theta(\mathbf{x}|\mathbf{z})p(\mathbf{z})$ this approach does not suffer from the decoder gradient problem. And since it uses a joint discriminator, it does not suffer from the multiple discriminators problem.

The idea of joint discriminators has been previously introduced in ALI (Dumoulin et al., 2016) and BIGAN (Donahue et al., 2016), who use the same discriminator in an adversarial setting.

6.3. Two baseline variants

To further explore the density ratio trick in variational inference, we compare with two other VAE-GAN hybrids. Like in Adversarial Auto-encoders, we replace the average KL term in Equation 3 with $\text{KL}[q_\eta(\mathbf{z})||p(\mathbf{z})]$ and use an observed likelihood, to obtain a reconstruction loss on data space. We add to the Adversarial Autoencoder setting a discriminator in data space to distinguish between reconstructions and data (this allows us to solve the one versus many discriminator problem, but not the lack of gradients - to solve this we add an adversarial loss to the decoder). We will call this variant AAE++. To determine how good AAE++ is at matching $q_\eta(\mathbf{z})$ and $p(\mathbf{z})$ via the density ratio trick, we also compare with a model (Rosca et al., 2017) where samples are classified as fake by the discriminator (using green line in Figure 3(e)). In AAE-GAN, the model learns to produce good samples without having to match $q_\eta(\mathbf{z})$ and $p(\mathbf{z})$ - though doing so will reduce the cost function. If this model substantially outperforms AAE++ we can conclude that the density ratio trick exhibits similar problems to the ones observed in Section 4 for standard VAEs: the marginal $q_\eta(\mathbf{z})$ and $p(\mathbf{z})$ are not matched, so areas with high mass in $p(\mathbf{z})$ are not covered by $q_\eta(\mathbf{z})$, which leads to bad samples.

These variants allow us to explore a wider spectrum in the VAE-GAN world and understand their limitations on real data experiments. However, they are harder to train: we noticed that it is hard for Adversarial Autoencoders to balance the adversarial loss trying to match $q(\mathbf{z})$ and $p(\mathbf{z})$ and the reconstruction loss - again, the inference-generation trade-off at play. To account for that, we introduce a coefficient for the data reconstruction loss both in AAE++ and AAE-GAN. For details, see Appendix 4.

6.4. Experimental results on adversarial and variational hybrids

We perform an extensive comparison between:

- VAEs with diagonal Gaussian posteriors as they are the most widespread variational inference model.
- DCGAN and WGAN-GP to provide a baseline for VAE-GAN hybrids.
- Adversarial autoencoders (AAE) to exhibit the effect of replacing the analytical KL in VAEs with the density ratio trick.
- VEEGAN to evaluate the density ratio trick performance on joint distributions, and the effect of having the reconstruction loss in latent space rather than data space.
- AAE++ enables us to see the effect of adding an adversarial loss on the reconstructions obtained using an Autoencoder GAN hybrid which uses the density ratio trick to force the marginal $q_{\eta}(\mathbf{z})$ to match the prior.
- AAE-GAN passes samples through a data discriminator, and from that perspective resembles a GAN. This variant allows for a direct comparison of hybrids against standard GAN models. Comparing AAE-GAN with AAE++ measures the ability of the density ratio trick to matching the marginal posterior distribution with the prior.

We do not compare with AdversarialVB, as it underperformed in our preliminary experiments (Appendix J). Other approaches to VAE-GAN hybrids include replacing reconstruction losses on pixels with reconstruction losses on discriminator features (Larsen et al., 2016), but those approaches are outside the scope of this work.

We train all models on three datasets: ColorMNIST (Metz et al., 2017), CelebA (Liu et al., 2015) and CIFAR-10 (Krizhevsky, 2009) and complement visual inspection of samples with three metrics: Inception Score, sample diversity, independent Wasserstein critic - these metrics are described in Appendix I. We present not only the best performing models, but also a box plot of hyperparameter sensitivity for each model in Figure 4 and Figure 5. We show model samples in Appendix H. Results show that VAEs perform well on datasets that have less variability, such as ColorMNIST and CelebA. However, they are not able to capture the subtleties of more complex datasets, like CIFAR10. GAN-

VAE hybrids can outperform both GANs and VAEs, but that is also dataset dependent. AAE-GAN consistently outperforms AAE++, showing that the density ratio trick has issues matching the marginal latent posterior to the prior. Matching marginal distribution, instead of conditional distributions can explain the increased sample quality of VAE-GAN hybrids compared to VAEs. GANs are a form on non-maximum likelihood learning, and the performance contrast shown by these results highlights the ongoing importance of the exploration for learning principles other than that of maximum likelihood.

Hyperparameters, network architectures and training details are discussed in Appendix K. All trained models are unconditional.

7. Practical implications

Avoiding the Inference-Generation trade-off: We have shown that there is a trade off between the inference and generation quality of a variational inference model. If a practitioner is mainly interested in sample quality, perhaps other models, such as GANs or PixelCNN (Goodfellow et al., 2014; van den Oord et al., 2016) would suffice. GANs are often criticized for being hard to train, and VAE-GAN hybrids are motivated as a stabilizing factor to avoid mode collapse. However, during this study we have found that these hybrids require carefully tuned loss coefficients and network architectures to match GANs on sample quality metrics. Moreover, some hybrids require novel architectures (such as joint or latent codes discriminator), for which there is less common wisdom compared to image architectures. We have also shown that the likelihood choice of VAEs can be a factor in the inference-generation trade-off: VAEs trained with a Bernoulli likelihood produce better samples, but worse reconstructions - see Section 4.2. Joint models such as VEEGAN circumvent problems with standard VAEs by using an observed likelihood on latent space and thus not relying on the observed likelihood for sample quality, but only as a stabilizing factor.

Divergence estimation and effects on bound tracking: The density ratio trick can be a useful tool for learning. However, it is not a reliable tool for divergence estimation. This has a direct effect on variational GAN hybrids: they lose a meaningful quantity for tracking training progress, as well as a tool to measure inference quality (plots in the Appendix, Section F). The effect of using the density ratio trick goes beyond bound tracking and can affect learning since as we have seen in Section 5, this approach does not scale well with data dimensionality.

Learning $q_{\eta}(\mathbf{z})$: We find that for continuous latent variables, learning the marginal posterior distribution is difficult, which has a direct effect on methods which learn the prior

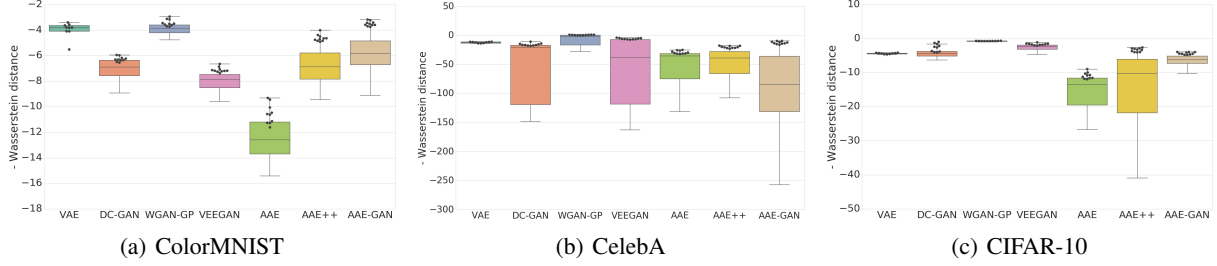


Figure 4. Best results (black dots) and hyperparameter sensitivity of negative Wasserstein distance estimated using an independent Wasserstein critic per model. Higher is better. The metric captures overfitting to the training data and low quality samples and been shown to correlate with human evaluations (Jiwoong Im et al., 2018).

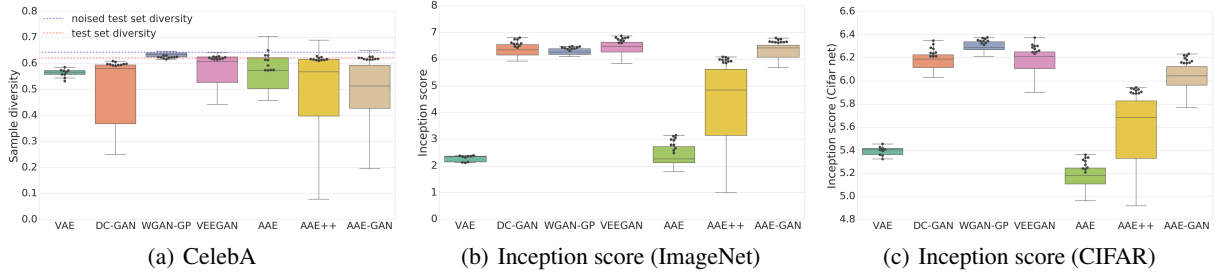


Figure 5. Left plot shows sample diversity results on CelebA. This measure needs to be viewed relative to test set: too much diversity means failure to capture the data distribution, too little is indicative of mode collapse. To illustrate this, we report the diversity obtained on a noised version of the test set (added normal noise with zero mean and 0.1 standard deviation), which leads to higher diversity than the test set. Middle plot: Inception score results on CIFAR-10. Right most plot shows Inception score computed using a VGG style network trained on CIFAR-10. For Inception scores, high values are better. The scores using samples from test data split were diversity: 0.621, inception score: 11.25, inception score (CIFAR-10 trained VGG net): 9.18. The best results obtained with each model are the black dots and hyperparameter sensitivity is given by the box plots. While not in this plot, DRAW obtained an Inception score of 3.37 using the Imagenet classifier and a 5.16 score using the CIFAR-10 classifier. To the best of our knowledge we are the first to report these numbers for DRAW. Upon acceptance we will open source the CIFAR10 classifier to make it available for others.

(Huang et al., 2017; Tomczak and Welling, 2017). While learning the prior can be difficult, it is a promising strategy for minimizing the gap between $q_\eta(\mathbf{z})$ and $p(\mathbf{z})$ in variational inference methods. We leave the analysis of these methods for future work.

Closest to our work, the inference–generation trade-off in latent variable models has been examined using rate-distortion analysis (Alemi et al., 2017), where rate is a measure of how well the aggregated posterior matches the prior and the distortion is a measure of reconstruction error. By introducing a coefficient in front of the KL term in the evidence lower bound (Higgins et al., 2017a) we can recover models with different points along the rate-distortion spectrum. By varying the complexity of the decoder and the encoder Alemi et al. (2017) show that deterministic feed-forward encoders have high rate and low distortion, whereas complex decoders have low rate and high distortion. Their work does not consider implicit encoders or decoders, and is complementary to our work which focuses on variational-GAN hybrids.

Conclusion: We showed there is a trade-off between inference and generation in variational inference methods. VAE-GAN hybrids offer the promise of addressing major challenges in variational inference, by using class probability estimation for marginal distribution minimization. Problems with value estimation of divergences, failures to scale to high dimensions and the struggles to outperform GANs on sample quality metrics show that implicit models and adversarial training did not solve the obstacles of VAE training. The limiting capacity of simple latent posteriors, challenges in divergence minimization and observation likelihoods remain issues to focus on when developing new variational inference models, with approaches that learn the prior, use marginal distribution matching and leverage complex but computationally cheap latent posteriors being promising avenues of research.

Acknowledgements We thank Danilo Rezende, Fabio Viola and Josh Abramson for helpful feedback and discussions.

References

- A. A. Alemi, B. Poole, I. Fischer, J. V. Dillon, R. A. Saurous, and K. Murphy. An information-theoretic analysis of deep latent-variable models. *arXiv preprint arXiv:1711.00464*, 2017.
- M. Arjovsky, S. Chintala, and L. Bottou. Wasserstein GAN. In *ICML*, 2017.
- D. M. Blei, A. Y. Ng, and M. I. Jordan. Latent Dirichlet allocation. *JMLR*, 2003.
- I. Danihelka, B. Lakshminarayanan, B. Uria, D. Wierstra, and P. Dayan. Comparison of Maximum Likelihood and GAN-based training of Real NVPs. *arXiv preprint arXiv:1705.05263*, 2017.
- J. Donahue, P. Krähenbühl, and T. Darrell. Adversarial feature learning. *arXiv preprint arXiv:1605.09782*, 2016.
- V. Dumoulin, I. Belghazi, B. Poole, A. Lamb, M. Arjovsky, O. Mastropietro, and A. Courville. Adversarially learned inference. *arXiv preprint arXiv:1606.00704*, 2016.
- R. Dutta, J. Corander, S. Kaski, and M. U. Gutmann. Likelihood-free inference by penalised logistic regression. *arXiv preprint arXiv:1611.10242*, 2016.
- M. C. Fu. Gradient estimation. *Handbooks in operations research and management science*, 13:575–616, 2006.
- I. Goodfellow, J. Pouget-Abadie, M. Mirza, B. Xu, D. Warde-Farley, S. Ozair, A. Courville, and Y. Bengio. Generative adversarial nets. In *NIPS*, 2014.
- I. J. Goodfellow. On distinguishability criteria for estimating generative models. *arXiv preprint arXiv:1412.6515*, 2014.
- K. Gregor, I. Danihelka, A. Graves, D. J. Rezende, and D. Wierstra. DRAW: A recurrent neural network for image generation. In *ICML*, 2015.
- K. Gregor, F. Besse, D. J. Rezende, I. Danihelka, and D. Wierstra. Towards conceptual compression. In *NIPS*, 2016.
- I. Gulrajani, F. Ahmed, M. Arjovsky, V. Dumoulin, and A. Courville. Improved Training of Wasserstein GANs. *arXiv preprint arXiv:1704.00028*, 2017.
- C. Guo, G. Pleiss, Y. Sun, and K. Q. Weinberger. On calibration of modern neural networks. *arXiv preprint arXiv:1706.04599*, 2017.
- I. Higgins, L. Matthey, A. Pal, C. Burgess, X. Glorot, M. Botvinick, S. Mohamed, and A. Lerchner. β -VAE: Learning basic visual concepts with a constrained variational framework. In *ICLR*, 2017a.
- I. Higgins, A. Pal, A. A. Rusu, L. Matthey, C. P. Burgess, A. Pritzel, M. Botvinick, C. Blundell, and A. Lerchner. DARLA: Improving zero-shot transfer in reinforcement learning. In *ICML*, 2017b.
- S. Hochreiter and J. Schmidhuber. Long short-term memory. *Neural computation*, 9(8):1735–1780, 1997.
- M. D. Hoffman and M. J. Johnson. ELBO surgery: yet another way to carve up the variational evidence lower bound. In *Workshop in Advances in Approximate Bayesian Inference, NIPS*, 2016.
- C.-W. Huang, A. Touati, L. Dinh, M. Drozdal, M. Havaei, L. Charlin, and A. Courville. Learnable explicit density for continuous latent space and variational inference. *arXiv preprint arXiv:1710.02248*, 2017.
- F. Huszár. Variational inference using implicit distributions. *arXiv preprint arXiv:1702.08235*, 2017.
- S. Ioffe and C. Szegedy. Batch normalization: Accelerating deep network training by reducing internal covariate shift. In *ICML*, 2015.
- D. Jiwoong Im, A. He Ma, G. W. Taylor, and K. Branson. Quantitatively evaluating GANs with divergences proposed for training. *ICLR*, 2018.
- T. Kim, M. Cha, H. Kim, J. Lee, and J. Kim. Learning to discover cross-domain relations with generative adversarial networks. *arXiv preprint arXiv:1703.05192*, 2017.
- D. Kingma and J. Ba. Adam: A method for stochastic optimization. *arXiv preprint arXiv:1412.6980*, 2014.
- D. P. Kingma and M. Welling. Auto-encoding variational Bayes. *arXiv preprint arXiv:1312.6114*, 2013.
- D. P. Kingma, S. Mohamed, D. J. Rezende, and M. Welling. Semi-supervised learning with deep generative models. In *NIPS*, 2014.
- D. P. Kingma, T. Salimans, R. Jozefowicz, X. Chen, I. Sutskever, and M. Welling. Improved variational inference with inverse autoregressive flow. In *NIPS*, 2016.
- A. Krizhevsky. Learning multiple layers of features from tiny images. 2009.
- A. B. L. Larsen, S. K. Sønderby, H. Larochelle, and O. Winther. Autoencoding beyond pixels using a learned similarity metric. In *Proceedings of The 33rd International Conference on Machine Learning*, pages 1558–1566, 2016.
- Z. Liu, P. Luo, X. Wang, and X. Tang. Deep learning face attributes in the wild. In *ICCV*, 2015.

- C. Louizos, U. Shalit, J. M. Mooij, D. Sontag, R. Zemel, and M. Welling. Causal effect inference with deep latent-variable models. In *Advances in Neural Information Processing Systems*, pages 6449–6459, 2017.
- A. L. Maas, A. Y. Hannun, and A. Y. Ng. Rectifier nonlinearities improve neural network acoustic models. In *ICML*, 2013.
- A. Makhzani, J. Shlens, N. Jaitly, I. Goodfellow, and B. Frey. Adversarial autoencoders. *arXiv preprint arXiv:1511.05644*, 2015.
- X. Mao, Q. Li, H. Xie, R. Y. Lau, Z. Wang, and S. P. Smolley. Least squares generative adversarial networks. *arXiv preprint ArXiv:1611.04076*, 2016.
- M. F. Mathieu, J. J. Zhao, J. Zhao, A. Ramesh, P. Sprechmann, and Y. LeCun. Disentangling factors of variation in deep representation using adversarial training. In *NIPS*, 2016.
- L. Mescheder, S. Nowozin, and A. Geiger. Adversarial Variational Bayes: Unifying Variational Autoencoders and Generative Adversarial Networks. In *ICML*, 2017.
- L. Metz, B. Poole, D. Pfau, and J. Sohl-Dickstein. Unrolled generative adversarial networks. In *ICLR*, 2017.
- S. Mohamed and B. Lakshminarayanan. Learning in implicit generative models. *arXiv preprint arXiv:1610.03483*, 2016.
- A. Nguyen, J. Yosinski, Y. Bengio, A. Dosovitskiy, and J. Clune. Plug & play generative networks: Conditional iterative generation of images in latent space. *arXiv preprint arXiv:1612.00005*, 2016.
- S. Nowozin, B. Cseke, and R. Tomioka. f -GAN: Training generative neural samplers using variational divergence minimization. *arXiv preprint arXiv:1606.00709*, 2016.
- A. Odena, C. Olah, and J. Shlens. Conditional image synthesis with auxiliary classifier GANs. *arXiv preprint arXiv:1610.09585*, 2016.
- G. Papamakarios, I. Murray, and T. Pavlakou. Masked autoregressive flow for density estimation. In *NIPS*, 2017.
- D. Rezende, I. Danihelka, K. Gregor, D. Wierstra, et al. One-shot generalization in deep generative models. In *International Conference on Machine Learning*, pages 1521–1529, 2016.
- D. J. Rezende and S. Mohamed. Variational inference with normalizing flows. In *ICML*, 2015.
- D. J. Rezende, S. Mohamed, and D. Wierstra. Stochastic backpropagation and approximate inference in deep generative models. In *ICML*, 2014.
- M. Rosca, B. Lakshminarayanan, D. Warde-Farley, and S. Mohamed. Variational approaches for auto-encoding generative adversarial networks. *arXiv preprint arXiv:1706.04987*, 2017.
- T. Salimans, I. Goodfellow, W. Zaremba, V. Cheung, A. Radford, and X. Chen. Improved techniques for training GANs. In *NIPS*, 2017.
- L. I. Smith. A tutorial on principal components analysis. Technical report, 2002.
- A. Srivastava, L. Valkov, C. Russell, M. Gutmann, and C. Sutton. VEEGAN: Reducing mode collapse in GANs using implicit variational learning. In *NIPS*, 2017.
- M. Sugiyama, T. Suzuki, and T. Kanamori. *Density ratio estimation in machine learning*. Cambridge University Press, 2012.
- C. Szegedy, V. Vanhoucke, S. Ioffe, J. Shlens, and Z. Wojna. Rethinking the inception architecture for computer vision. In *CVPR*, 2016.
- L. Theis, A. van den Oord, and M. Bethge. A note on the evaluation of generative models. In *ICLR*, 2016.
- I. Tolstikhin, O. Bousquet, S. Gelly, and B. Schoelkopf. Wasserstein auto-encoders. In *ICLR*, 2018.
- J. M. Tomczak and M. Welling. VAE with a VampPrior. *arXiv preprint arXiv:1705.07120*, 2017.
- A. van den Oord, N. Kalchbrenner, L. Espeholt, O. Vinyals, A. Graves, et al. Conditional image generation with pixel CNN decoders. In *NIPS*, 2016.
- A. van den Oord, O. Vinyals, and K. Kavukcuoglu. Neural discrete representation learning. In *NIPS*, 2017.
- Z. Wang, E. P. Simoncelli, and A. C. Bovik. Multiscale structural similarity for image quality assessment. In *Conference Record of the Thirty-Seventh Asilomar Conference on Signals, Systems and Computers, 2004.*, volume 2, pages 1398–1402. IEEE, 2003.
- S. N. Wood. Statistical inference for noisy nonlinear ecological dynamic systems. *Nature*, 466(7310):1102–1104, 2010.
- J. Zhao, M. Mathieu, and Y. LeCun. Energy-based generative adversarial network. In *ICLR*, 2017.
- J.-Y. Zhu, T. Park, P. Isola, and A. A. Efros. Unpaired image-to-image translation using cycle-consistent adversarial networks. *arXiv preprint arXiv:1703.10593*, 2017.

Appendix

A. Estimating $\text{KL}[q_\eta(\mathbf{z})||p(\mathbf{z})]$: experimental details

In this section we present the details of marginal KL estimation experiments described in detail in Section 4.

A.1. Trained variational models

For the experiments presented in Table 1, we trained standard VAEs and a DRAW model to minimize the evidence lower bound. The VAEs were trained using a Bernoulli visible distribution and a diagonal Gaussian posterior. The architectures are the ones reported in Appendix K. The DRAW model was similar to the one described in the original paper (Gregor et al., 2015) and obtained less than 3.67 bits/pixel. For comparison with other models - see Figure 5, DRAW obtained an Inception score of 3.37 and a 5.16 score using the CIFAR-10 classifier. To the best of our knowledge we are the first to report these numbers for DRAW.

A.2. Estimating $\text{KL}[q_\eta(\mathbf{z})||p(\mathbf{z})]$ using the Monte Carlo approach

Algorithm 1 describes the approach used to estimate $\text{KL}[q_\eta(\mathbf{z})||p(\mathbf{z})]$ via Monte Carlo methods. While this approach is computationally expensive, it is the most accurate one. We now describe the details of this computation. For each x_i we used 10^6 samples from $q(z|x)$ to estimate $\log \frac{q_\eta(\mathbf{z})}{p(\mathbf{z})}$. To estimate $q_\eta(\mathbf{z})$ for latent sample we used the entire dataset training and validation split of the dataset at hand. In all our figures and tables, this number is reported as N .

Algorithm 1 Pseudocode for estimating the marginal KL using MC

```

1: Load trained variational model with prior  $p(\mathbf{z})$ , and
   posterior  $q_\eta(\mathbf{z}|\mathbf{x})$ .
2: marginal_kl = 0.0
3: for  $i = 1 : \text{num\_z}$  do
4:   sample  $x_i$  from  $p^*(\mathbf{x})$ , sample  $z_i$  from  $q_\eta(\mathbf{z}|x_i)$ 
5:   posterior_list = []
6:   for  $\mathbf{x}$  in dataset do
7:     append  $\log q_\eta(\mathbf{z}|\mathbf{x})(z_i)$  to posterior_list
8:   end for
9:    $\log q(z_i) = \log \text{sum\_exp}(\text{posterior\_list})$ 
10:   $\text{marginal\_kl} += \log q(z_i) - \log p(z_i)$ 
11: end for
12:  $\text{marginal\_kl} = \text{marginal\_kl} / \text{num\_z}$ 

```

A.3. Estimating $\text{KL}[q_\eta(\mathbf{z})||p(\mathbf{z})]$ using the density ratio trick

To estimate $\text{KL}[q_\eta(\mathbf{z})||p(\mathbf{z})]$ using the density ratio trick, we used Algorithm 2. For all datasets, we noticed that this

approach is highly sensitive to hyperparameters. We explain this two fold: First, this approach relies on the probabilities reported by a neural network classifier, which have been known to be inaccurate. New methods have been proposed to address this issue Guo et al. (2017), and we leave exploring these approaches for future work. Second, as shown in Section A.4, the distribution $q(z)$ can be very complex, making it hard for the classifier to learn to distinguish between samples from the two distributions.

We show the hyperparameter sensitivity by training different models to estimate the marginal $\text{KL}[q_\eta(\mathbf{z})||p(\mathbf{z})]$ for the same VAE and report the different values obtained. All trained density ratio estimators were MLPs with Leaky Rectified activations of slope 0.2 and were trained for $5 * 10 * 5$ steps using the AdamOptimizer with β_1 and β_2 equal to 0.9.

Results on ColorMNIST are summarized in Table 2, while CelebA results are summarized in Table 3.

While analyzing these results, we observed that adding noise to the activation of the classifier resulted in a better classifier, but also a more confident one, which underestimates the probability that a sample was given by the prior, and the KL value being over estimated. We also see that the resulting KL is quite sensitive to the architecture of the classifier, with an extra layer resulting in a substantial value increase for the Color MNIST case. Gradients penalties and dropout did not result in a big change in the estimated value.

Algorithm 2 Pseudocode for estimating the marginal KL using the density ratio trick

```

1: Load trained variational model with prior  $p(\mathbf{z})$ , and
   posterior  $q_\eta(\mathbf{z}|\mathbf{x})$ .
2: Initialize code discriminator parameters  $\omega$  randomly.
3: for iter = 1 : max_iter do
4:   Update parameters  $\omega$  by maximizing
      $\mathbb{E}_{p^*(\mathbf{x})} \mathbb{E}_{q_\eta(\mathbf{z}|\mathbf{x})} [\log \mathcal{C}_\omega(\mathbf{z})] + \mathbb{E}_{p(\mathbf{z})} [\log(1 - \mathcal{C}_\omega(\mathbf{z}))]$ 
5: end for
6: marginal_kl = 0.0
7: for  $i = 1 : \text{num\_z}$  do
8:   sample  $x_i$  from  $p^*(\mathbf{x})$ , sample  $z_i$  from  $q_\eta(\mathbf{z}|x_i)$ 
9:    $\text{marginal\_kl} += \log \mathcal{C}_\omega(z_i) - \log(1 - \mathcal{C}_\omega(z_i))$ 
10: end for
11:  $\text{marginal\_kl} = \text{marginal\_kl} / \text{num\_z}$ 

```

A.4. Estimating $\text{KL}[q_\eta(\mathbf{z})||p(\mathbf{z})]$ using a density model for $q(z)$

We now explore the challenges of learning the marginal $q(z)$ using three density models: Gaussian Mixture Model, Masked Auto-regressive Flows (Papamakarios et al., 2017), and Gaussian auto-regressive models implemented using an (Hochreiter and Schmidhuber, 1997). Algorithm 3 was used to learn these models.

Table 2. Estimating a marginal KL using the density ratio trick for a standard VAE with 50 latents trained on Color MNIST. The number of hidden units per layer was 5000. When the KL is estimated numerically, the result is 12.3. From equation (5) and that the mutual information term is bound by $\log N$, with $N = 60000$ and the average posterior KL of the model is 23.34, we know that the value needs to be greater than 12.46. All models used a learning rate of 0.0005.

| # layers | Gradient Penalty | Activation Noise | KL |
|----------|------------------|------------------|---------|
| 3 | No | No | 2.3 |
| 4 | No | No | 3.3 |
| 4 | No | Yes | 25812.8 |
| 4 | Yes | No | 3.05 |

Table 3. Estimating a marginal KL using the density ratio trick for a standard VAE with 100 latents trained on CelebA. The number of hidden units per layer was 5000. When the KL is estimated numerically, the result is 100.3. From equation (5) and that the mutual information term is bound by $\log N$, with $N = 162770$ and the average posterior KL of the model is 112.37, we know that the value needs to be greater than 100.0.

| # layers | Learning Rate | Activation Noise | Dropout | KL |
|----------|---------------|------------------|---------|------------|
| 5 | 0.0005 | No | No | 17.74 |
| 5 | 0.0005 | Yes | No | 720140.922 |
| 5 | 0.0001 | No | No | 14.83 |
| 7 | 0.0005 | No | No | 18.82 |
| 7 | 0.0005 | No | Yes | 19.01 |
| 7 | 0.0001 | No | No | 18.02 |
| 10 | 0.0001 | No | No | 18.12 |

Diagonal Gaussian Mixture Models:

In this setting, we model $q_\eta(\mathbf{z})$ using:

$$q_\eta(\mathbf{z}) = \sum_i^k \pi_i \mathcal{N}(\mathbf{z} | \mu_i, \sigma_i), \sum_i^k \pi_i = 1$$

The number of mixtures is a hyperparameter, and we tried 10, 50 and 100. The models were trained using the Adam Optimizer, with learning rates in $1e-4$, $5e-4$, $1e-3$, $5e-5$.

Masked Auto-regressive Flows:

In this setting, the density model is given by transforming a standard Gaussian using auto-regressive models as normalizing flows:

$$q_\eta(\mathbf{z}) = \mathcal{N}(0, \mathbb{I} | \mathbf{z}) \left| \det \left(\frac{d f^{-1}}{dz} \right) \right|$$

where f has to be an invertible function for which the determinant of its Jacobian is easy to compute. In practice, we leverage the fact that the composition of two functions which have these proprieties also has this property to chain a number of transforms.

We trained models with a ranging number of flows (from 1 to 3), and different layer sizes (512, 1024 or 2048) and number of layers per flow (1 or 2). The models were trained using the Adam Optimizer, with learning rates in $1e-4$, $5e-4$, $1e-3$.

Gaussian Auto-regressive models:

The auto-regressivity of the recurrent neural network was used to model $q(z_i | z_{<i})$:

$$q_\eta(\mathbf{z}) = \prod q(z_i | z_{<i}) = \prod \mathcal{N}(z_i | \mu(z_{<i}), \sigma(z_{<i}))$$

We trained models with different number of recurrent layers, ranging from 1 to 5, and hidden units in 500, 1000, 200. The models were trained using the Adam Optimizer, with learning rates in $1e-4$, $5e-4$, $1e-3$, $5e-5$. The best performing models had 3 recurrent layer, with a consistent benefit seen going from 1 layer to 2 layers and 3 layers, but no benefits in further layers.

Algorithm 3 Pseudocode for estimating the marginal KL using a density estimator for $q(\mathbf{z})$

- 1: Load trained variational model with prior $p(\mathbf{z})$, and posterior $q_\eta(\mathbf{z} | \mathbf{x})$.
- 2: Initialize density \mathbf{t} model parameters ω randomly.
- 3: **for** iter = 1 : max_iter **do**
- 4: Update parameters ω by maximizing $\mathbb{E}_{p^*(\mathbf{x})} \mathbb{E}_{q_\eta(\mathbf{z} | \mathbf{x})} [\log(\mathbf{t}(\mathbf{z}))]$
- 5: **end for**
- 6: marginal_kl = 0.0
- 7: **for** i = 1 : num_z **do**
- 8: sample x_i from $p^*(\mathbf{x})$, sample z_i from $q_\eta(\mathbf{z} | x_i)$
- 9: marginal_kl += $\log(\mathbf{t}(z_i)) - \log p(z_i)$
- 10: **end for**
- 11: marginal_kl = marginal_kl / num_z

Results: A comparison between the best performing model from each family on ColorMNIST and CIFAR10 is presented in Figure 6. Within the same model family, we observed (unsurprisingly) that Gaussian Mixture Models perform better with more mixtures, bigger LSTMs (more layers and more units per layers) perform better, though training more did not help. However, scaling Masked Auto-regressive Flows was not as simple, with a higher number of transforms often resulting in divergence.

B. Augmenting the ELBO with

KL $[q_\eta(\mathbf{z}) || p(\mathbf{z})]$ via the density ratio trick

We have shown that VAEs trained to maximize the variational lower bound do not succeed in $\text{KL}[q_\eta(\mathbf{z}) || p(\mathbf{z})]$, and that the density ratio trick can be successfully used to provide gradients for learning. A natural question would then be: can we improve VAEs by adding an extra term which

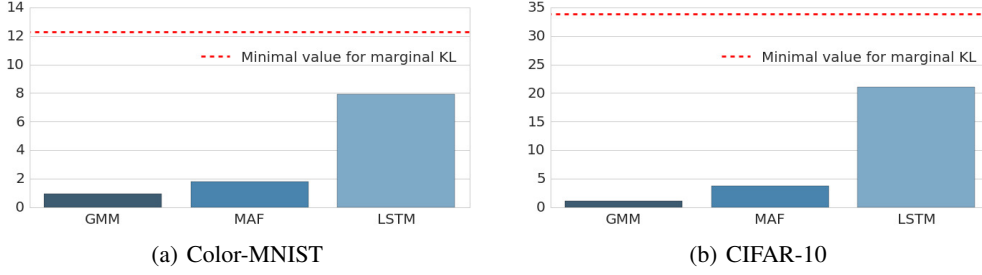


Figure 6. Estimating $\text{KL}[q_\eta(\mathbf{z})||p(\mathbf{z})]$ using different density models to estimate $q(z)$: Gaussian Mixture Models (GMM), Masked Auto-regressive Flow (MAF) and LSTMs. We plot the minimal value for the marginal KL - computed from equation 5 - which allows us to conclude that all three density estimation approaches underestimate the true KL. We observe that for both datasets, LSTMs outperform the other models, showing that the autoregressivity of these models is necessary to model $q_\eta(\mathbf{z})$.

directly minimizes $\text{KL}[q_\eta(\mathbf{z})||p(\mathbf{z})]$ via the density ratio trick?

We have trained models to maximize:

$$\mathbb{E}_{p^*(\mathbf{x})} [E_{q_\eta(\mathbf{z}|\mathbf{x})} [\log p_\theta(\mathbf{x}|\mathbf{z})] - \text{KL}[q_\eta(\mathbf{z}|\mathbf{x})||p(\mathbf{z})]] - \lambda \text{KL}[q_\eta(\mathbf{z})||p(\mathbf{z})]$$

We used the parameter λ to analyze the effect of the additional cost. Detailed results on models trained on ColorMNIST are in Table 4. The conclusion we draw in this case is that adding the marginal KL did improve, but not significantly. Perhaps results can be improved by additional tuning of λ or the discriminator network, since as we have seen throughout this paper, the success of the density ratio trick is dependent on careful tuning. Another explanation for these results can be given by the difficulty of optimizing multiple losses via the prevailing optimization methods.

| λ | Avg. posterior KL | MC estimated marginal KL |
|-----------|-------------------|--------------------------|
| 0 | 23.4 | 12.2 |
| 1 | 22.52 | 11.57 |
| 2 | 22.34 | 11.4 |
| 10 | 22.23 | 11.29 |

Table 4. Estimated marginal KL divergences for VAEs with a cost function augmented with $\text{KL}[q_\eta(\mathbf{z})||p(\mathbf{z})]$. The number of latents used was 50.

C. AAE-GAN loss function and pseudocode

In all the equations below, D_θ refers to the data discriminator, while \mathcal{C}_ω refers to the code discriminator. They are both trained to minimize a cross entropy loss, like in the original GAN formulation.

The loss function for AAE++ is:

$$\mathbb{E}_{q_\eta(\mathbf{z}|\mathbf{x})} \left[-\lambda \|\mathbf{x} - \mathcal{G}_\theta(\mathbf{z})\|_1 + \log \frac{\mathcal{D}_\phi(\mathcal{G}_\theta(\mathbf{z}))}{1 - \mathcal{D}_\phi(\mathcal{G}_\theta(\mathbf{z}))} + \log \frac{\mathcal{C}_\omega(\mathbf{z})}{1 - \mathcal{C}_\omega(\mathbf{z})} \right] \quad (10)$$

In contrast, the loss function for AAE-GAN is:

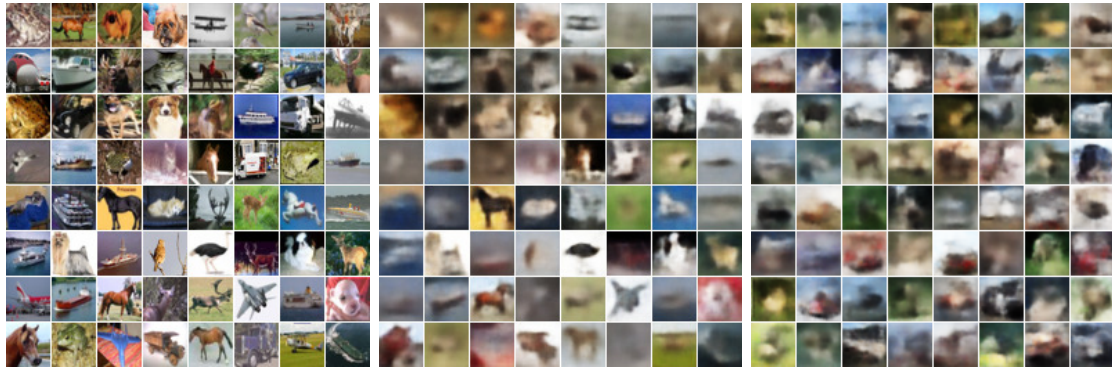
$$\mathbb{E}_{q_\eta(\mathbf{z}|\mathbf{x})} \left[-\lambda \|\mathbf{x} - \mathcal{G}_\theta(\mathbf{z})\|_1 + \log \frac{\mathcal{D}_\phi(\mathcal{G}_\theta(\mathbf{z}))}{1 - \mathcal{D}_\phi(\mathcal{G}_\theta(\mathbf{z}))} + \log \frac{\mathcal{C}_\omega(\mathbf{z})}{1 - \mathcal{C}_\omega(\mathbf{z})} \right] + \mathbb{E}_{p(\mathbf{z})} \log \frac{\mathcal{D}_\phi(\mathcal{G}_\theta(\mathbf{z}))}{1 - \mathcal{D}_\phi(\mathcal{G}_\theta(\mathbf{z}))} \quad (11)$$

The overall training procedure is summarized in Algorithm 4.

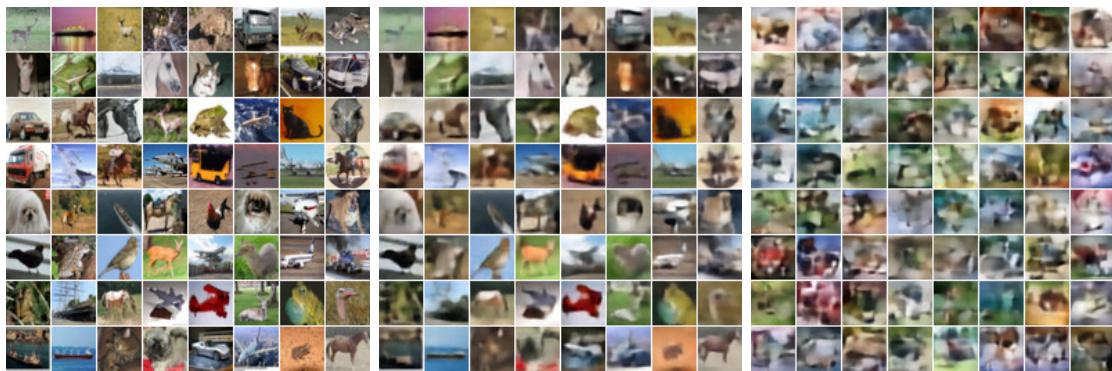
D. The effect of the pixel distribution on the Inference-Generation trade off in VAE training

Figure 7 visually shows the trade-off seen between using a Bernoulli or a QuantizedNormal distribution as the visible pixel distribution, $p(\mathbf{x}|\mathbf{z})$ in VAEs.

We now unpack the mathematical justification for why the Bernoulli distribution produces worse reconstructions. We will perform the analysis for a pixel x , but this straightforwardly extends to entire images. Assume a Bernoulli distribution with mean $\mu \in [0, 1]$. Then the Bernoulli loss is $x\mu - \log(1 + e^\mu)$. The gradient of the loss is $x - \sigma(\mu)$, where σ is the sigmoid function. If we use a Gaussian distribution with mean m and standard deviation s , the gradient is $\frac{x-m}{s^2}$. We can see that the gradients of the two distributions have the same form, and using a Bernoulli distribution is equivalent to using a Gaussian distribution with variance 1. By setting the variance to 1, using a Bernoulli likelihoods spreads mass around each pixel and cannot specialize to produce good reconstructions.



(a) Bernoulli



(b) Quantized Normal

Figure 7. Comparisons of reconstructions and samples generated from VAEs using Bernoulli and Quantized Normal pixel distributions. The observed trade-off between reconstruction and sample quality is consistent throughout different hyperparameters. For the models displayed here, the difference can be seen in the different KL values obtained in the loss function used to train the models: 44.7 for the Bernoulli model, and 256.7 for the QuantizedNormal model.

Algorithm 4 Pseudocode for AAE-GAN

- 1: Initialize parameters of generator θ , encoder η , discriminator ϕ and code discriminator ω randomly.
- 2: Let $\hat{\mathbf{z}} \sim q_\eta(\mathbf{z}|\mathbf{x})$ denote a sample from $q_\eta(\mathbf{z}|\mathbf{x})$ and $\hat{\mathbf{x}} = \mathcal{G}_\theta(\hat{\mathbf{z}})$ denote the ‘reconstruction’ of \mathbf{x} using $\hat{\mathbf{z}}$.
- 3: Let $R_{\mathcal{D}_\phi}(\mathbf{x}) = -\log \mathcal{D}_\phi(\mathbf{x}) + \log(1 - \mathcal{D}_\phi(\mathbf{x}))$
- 4: Let $R_{\mathcal{C}_\omega}(\mathbf{z}) = -\log \mathcal{C}_\omega(\mathbf{z}) + \log(1 - \mathcal{C}_\omega(\mathbf{z}))$
- 5: **for** iter = 1 : max_iter **do**
- 6: Update encoder η by minimizing

\triangleright data reconstruction and code generation loss

$$\mathbb{E}_{p^*(\mathbf{x})} \mathbb{E}_{q_\eta(\mathbf{z}|\mathbf{x})} [\lambda \|\mathbf{x} - \mathcal{G}_\theta(\mathbf{z})\|_1 + R_{\mathcal{C}_\omega}(\mathbf{z})] \approx \mathbb{E}_{p^*(\mathbf{x})} [\lambda \|\mathbf{x} - \hat{\mathbf{x}}\|_1 + R_{\mathcal{C}_\omega}(\hat{\mathbf{z}})] \quad (12)$$

- 7: Update generator θ by minimizing

\triangleright data reconstruction and generation loss

$$\begin{aligned} & \mathbb{E}_{p^*(\mathbf{x})} \mathbb{E}_{q_\eta(\mathbf{z}|\mathbf{x})} [\lambda \|\mathbf{x} - \mathcal{G}_\theta(\mathbf{z})\|_1 + R_{kl}(\mathbf{z})] + \mathbb{E}_{p(\mathbf{z})} [R_{\mathcal{D}_\phi}(\mathcal{G}_\theta(\mathbf{z}))] \\ & \approx \mathbb{E}_{p^*(\mathbf{x})} [\lambda \|\mathbf{x} - \hat{\mathbf{x}}\|_1 + R_{\mathcal{D}_\phi}(\hat{\mathbf{x}})] + \mathbb{E}_{p(\mathbf{z})} [R_{\mathcal{D}_\phi}(\mathcal{G}_\theta(\mathbf{z}))] \end{aligned}$$

- 8: Update discriminator ϕ by minimizing

\triangleright treat data as real, reconstructions and samples as fake

$$\begin{aligned} & \mathbb{E}_{p^*(\mathbf{x})} [-2 \log \mathcal{D}_\phi(\mathbf{x}) - \mathbb{E}_{q_\eta(\mathbf{z}|\mathbf{x})} \log(1 - \mathcal{D}_\phi(\mathcal{G}_\theta(\mathbf{z})))] + \mathbb{E}_{p(\mathbf{z})} [-\log(1 - \mathcal{D}_\phi(\mathcal{G}_\theta(\mathbf{z})))] \\ & \approx \mathbb{E}_{p^*(\mathbf{x})} [-\log \mathcal{D}_\phi(\mathbf{x}) - \log(1 - \mathcal{D}_\phi(\hat{\mathbf{x}}))] + \mathbb{E}_{p(\mathbf{z})} [-\log(1 - \mathcal{D}_\phi(\mathcal{G}_\theta(\mathbf{z})))] \end{aligned}$$

- 9: Update code discriminator ω by minimizing

\triangleright treat $p(\mathbf{z})$ as real and codes from the encoder as fake

$$\mathbb{E}_{p^*(\mathbf{x})} \mathbb{E}_{q_\eta(\mathbf{z}|\mathbf{x})} [-\log(1 - \mathcal{C}_\omega(\mathbf{z}))] + \mathbb{E}_{p(\mathbf{z})} [-\log \mathcal{C}_\omega(\mathbf{z})] \approx \mathbb{E}_{p^*(\mathbf{x})} [-\log(1 - \mathcal{C}_\omega(\hat{\mathbf{z}}))] + \mathbb{E}_{p(\mathbf{z})} [-\log(\mathcal{C}_\omega(\mathbf{z}))] \quad (13)$$

10: **end for**

E. Density ratio synthetic experiments on Gaussian distributions

In this section we detail the experiments performed on density estimation on Gaussians. More results are presented in Figures 8 and 9. The discriminator was trained with the AdamOptimizer with β_1 set to 0.5, for 1000000 iterations. The results in Figure 2 were obtained using a 4 layer MLP, trained with a learning rate of 0.0001. The learning rate used for learning the Gaussian was 0.001. Similar results were obtained for different learning rates for the discriminator and the linear model of the Gaussian distribution.

F. Tracking the variational lower bound during training

In this section we compare the evidence lower bound training behavior, between VAEs, and a VAE-GAN hybrid, VEEGAN. VEEGAN introduces a new bound,

$$\text{KL}[p_\theta(\mathbf{x}|\mathbf{z})p(\mathbf{z})||p_\gamma(\mathbf{z}|\mathbf{x})p(\mathbf{x})] - \mathbb{E}[\log(p(\mathbf{z}))] + l_1(\mathbf{z}, F_\theta(\mathbf{x})) \quad (14)$$

where F_θ is the reconstructor network used to build the implicit $p(\mathbf{x}|\mathbf{z})$ and the KL divergence is estimated using the density ratio trick. The expected and desired behavior is that the bound increases as training progresses, however, as

seen in Figure 11, variational hybrids do not solve one of the fundamental problems with adversarial model training, namely introducing a quantity to use to assess convergence. Throughout this paper we have shown that the density ratio trick cannot be used to approximate KL divergences, and this is reflected in the estimated bounds of VAE-GAN hybrids, including VEEGAN.

Similar results were obtained using AdversarialVB in a maximum likelihood setting - see Figure 18 in [Daniehelka et al. \(2017\)](#).

G. Reconstructions

We show reconstructions obtained using AAE-GAN and VAEs for the CelebA dataset in Figure 12 and on CIFAR-10 in Figure 13.

H. Model samples for real data experiments

We show samples obtained on CelebA, CIFAR10 and ColorMNIST in Figures 14, 15 and 16, respectively.

I. Real data evaluation metrics

A universal metric that can assess both overfitting, sample quality and sample diversity has not been found for generative models. Instead, multiple metrics which assess

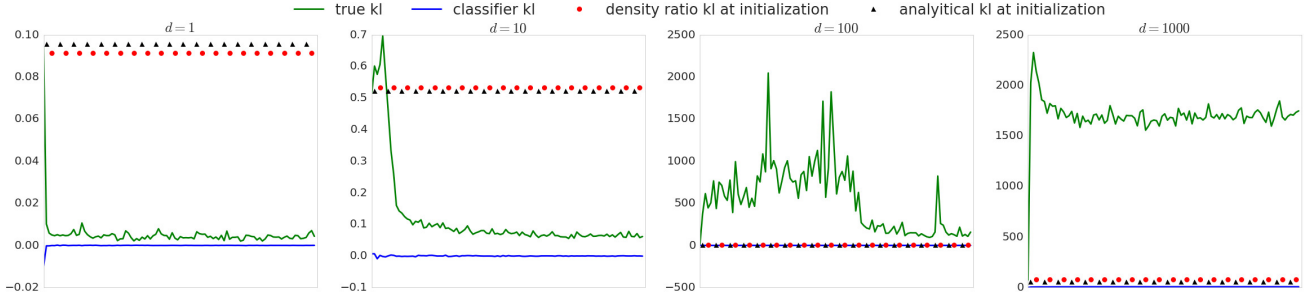


Figure 8. Results obtained on the synthetic Gaussian experiments, for data different dimensions d , with a smaller discriminator net (3 layers). We plot how the training progresses by evaluating the true KL divergence between the learned model and the data distribution. For comparison, we plot the true KL divergence at initialization, together with how well the same discriminator architecture is able to estimate the initial true KL when the two Gaussian distributions are fixed, and the two Gaussian distributions are stationary. The learning rate used for learning the Gaussian was 0.001. The discriminator learning rate was 0.0001. We can see that for lower dimensional data (1 and 10 dimensions), the model is able to decrease the true KL divergence between the learned Gaussian distribution and the true distribution. However, for higher dimensional Gaussians (dimensions 100 and 1000), the discriminator with 100 million parameters is not able to provide useful gradients and learning diverges. Results are averaged over 10 different initializations for the discriminator.

different aspects of a model have been proposed. To get a better overview of model performance, we use metrics which each capture a different aspect of training.

Inception score - sample quality and between class sample diversity: The most popular evaluation metric for implicit models is the Inception Score (Salimans et al., 2017). The Inception Score correlates with human sample evaluation and measures sample quality, between class sample diversity, but cannot capture within class mode collapse (for example, the model could generate the same horse again and again, and the Inception Score will not penalize it) or overfitting. The Inception score uses the last layer logits of a ImageNet trained Inception network (Szegedy et al., 2016) to determine how classifiable a sample is. For generative models trained on CIFAR10, we complement our reporting by using a VGG style convolutional neural network, trained on CIFAR10, which obtained 5.5% error. We will open source this classifier, to make it available for others to use.

Multi-scale structural similarity (MS-SSIM): sample diversity: To measure sample diversity, we use 1.0 - MS-SSIM (Wang et al., 2003), an image similarity metric ranging between 0.0 (low similarity) and 1.0 (high similarity) that has been shown to correlate well with human judgment. The use of MS-SSIM for sample diversity was introduced by Odena et al. (2016), which used it to compute in class sample similarity for conditional models, as between class variability can lead to ambiguous results. For models trained on the CelebA dataset, we can use this sample diversity metric, since the dataset only contains faces.

Independent Wasserstein critic - sample quality and overfitting: Danihelka et al. (2017) and Jiwoong Im et al. (2018) proposed training an independent Wasserstein GAN critic to distinguish between real data and generated samples.

This metric has been shown to correlate with human evaluations (Jiwoong Im et al., 2018), and if the independent critic is trained on validation data, it can also be used to measure overfitting (Danihelka et al., 2017). All our reported results using the Independent Wasserstein Critic use a WGAN-GP model, trained to distinguish between the data validation set and model samples.

J. AdversarialVB results

Results obtained using AdversarialVB are presented in Figure 17.

K. Training details: hyperparameters and network architectures

For all our models, we kept a fixed learning rate throughout training. We note the difference with AGE, where the authors decayed the learning rate during training, and changed the loss coefficients during training¹. The exact learning rate sweeps are defined in Table 5. We used the Adam optimizer (Kingma and Ba, 2014) with $\beta_1 = 0.5$ and $\beta_2 = 0.9$ and a batch size of 64 for all our experiments. We used batch normalization (Ioffe and Szegedy, 2015) for all our experiments. We trained all ColorMNIST models for 100000 iterations, and CelebA and CIFAR-10 models for 200000 iterations.

K.1. Scaling coefficients

We used the following sweeps for the models which have combined losses with different coefficients (for all our base-

¹As per advice found here: <https://github.com/DmitryUlyanov/AGE/>

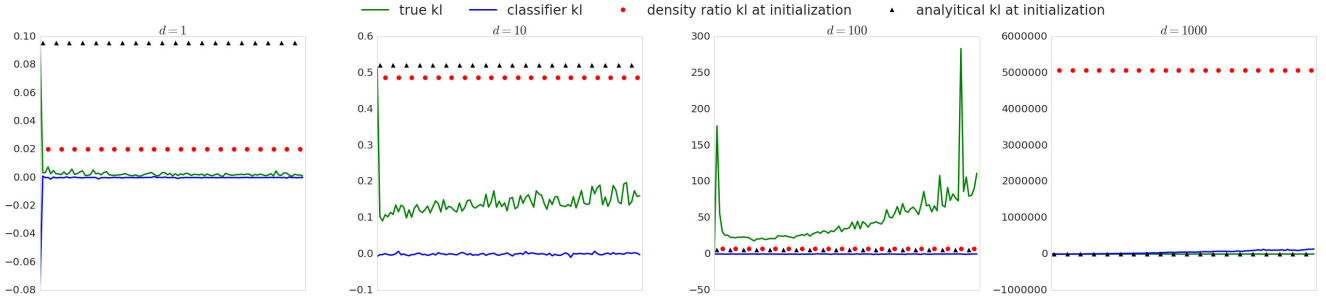


Figure 9. Results obtained on the synthetic Gaussian experiments, for data different dimensions d , **with a higher learning rate for the discriminator: 0.001**. We plot how the training progresses by evaluating the true KL divergence between the learned model and the data distribution. For comparison, we plot the true KL divergence at initialization, together with how well the same discriminator architecture is able to estimate the initial true KL when the two Gaussian distributions are fixed, and the two Gaussian distributions are stationary. The learning rate used for learning the Gaussian was 0.001. We can see that for lower dimensional data (1 and 10 dimensions), the model is able to decrease the true KL divergence between the learned Gaussian distribution and the true distribution. For 100 dimensional Gaussians, we see that learning the model distribution results in divergence, while for 1000 dimensional Gaussians we see that estimating the KL divergence between the initial Gaussians results in divergence. Results are averaged over 10 different initializations for the discriminator.

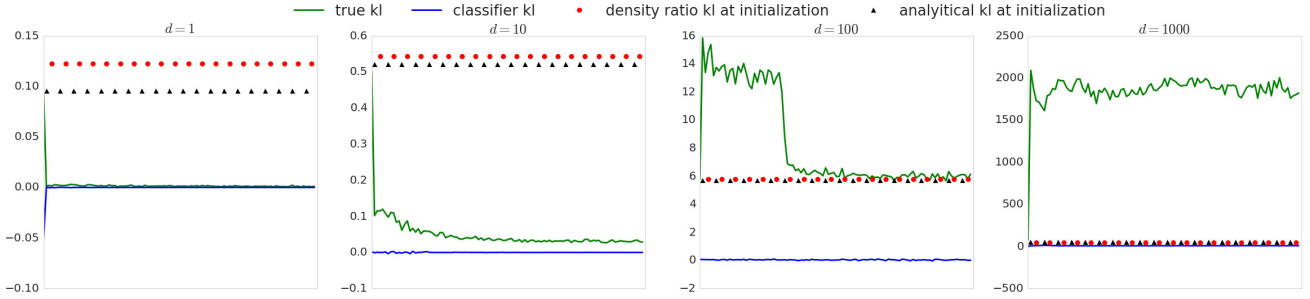


Figure 10. Results obtained on the synthetic Gaussian experiments, for data different dimensions d , **with 5 discriminator updates**. This figure is the analogous of Figure 2 - the experimental set up is exactly the same, including seeds and hyperparameters but the discriminator is updated 5 times per generator update. We notice that making the discriminator updates more frequent makes the learned model converge earlier for $d = 1, 10, 100$ but no improvement for $d = 1000$. However, we see no improvement in the estimated KL, even in cases where the discriminator could estimate the KL when trained to optimality, reported as 'density ratio KL as initialization'. The discriminator learning rate was 0.0001.

lines, we took the sweep ranges from the original papers):

- WGAN-GP
 - The gradient penalty of the discriminator loss function: 10.
- AAE-GAN and AAE++
 - Data reconstruction loss for the encoder: sweep over 1, 5, 10, 50.
 - Data reconstruction loss for the generator: sweep over 1, 5, 10, 50.
 - Adversarial loss for the generator (coming from the data discriminator): 1.0.
 - Adversarial loss for the encoder (coming from the code discriminator): 1.0.

For Adversarial Autoencoders and VEEGAN, we followed the advice from the original paper and did not weight the different loss terms using coefficients.

K.2. Choice of loss functions

For VEEGAN, we used the l_1 loss as the code reconstruction loss. For AAE++ and AAE-GAN, we used l_1 as the data reconstruction loss and the classifier GAN loss for the data and code discriminator.

K.3. Updates

For the WGAN-GP experiments, we did 5 discriminator updates for generator update. All other models used the same number updates for model component (discriminator, generator, encoder, decoder).

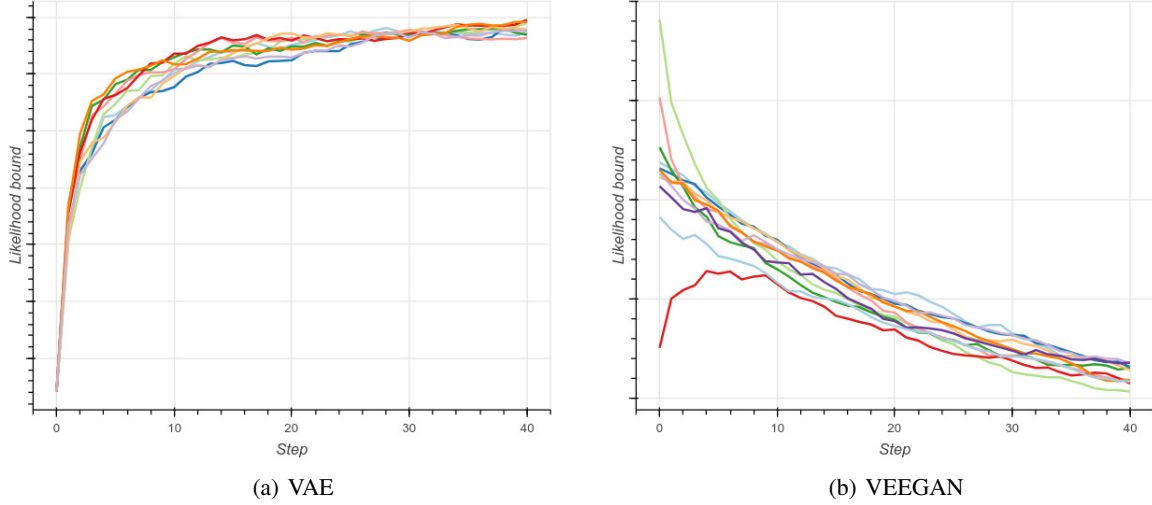


Figure 11. Training curves of the variational lower bound of a standard VAE with Bernoulli visible distribution (left) and VEEGAN (right) across different models trained. All results were obtained on CIFAR-10. We note that since the bound of VEEGAN is not obtained on the observed data (equation 14), the numbers are not directly comparable. The aim of this plot is to show the **trend** of training, as we expect that as model training progresses, the likelihood increases. We see that for VEEGAN this is not the case, even though the models perform comparable with state of the art (see Figure 5). Our investigation shows that for VEEGAN the adversarial loss goes up, even when the model improves. These results are not surprising given the results obtained on Gaussian distributions (Figures 2, 9 and 10), where we have seen that even when the density ratio trick provides useful gradients for learning, it severely underestimates the true divergence.

| Network | VAE | DCGAN WGAN-GP | AAE | AAE++ AAE-GAN | VEEGAN |
|--------------------|----------------------|------------------------|--------------------------|------------------|-----------------|
| Generator/Encoder | 0.001, 0.0005, 0.005 | 0.0001, 0.0002, 0.0003 | 0.001, 0.0005, 0.005 | 0.0001, 0.0005 | 0.001, 0.0005 |
| Discriminator | — | 0.0001, 0.0002, 0.0003 | — | 0.0005 | 0.00005, 0.0001 |
| Code discriminator | — | — | 0.0005, 0.00005, 0.00001 | 0.0005 | — |

Table 5. Learning rate sweeps performed for each model.

K.4. Choice of latent prior

We use a univariate normal prior for all models.

K.5. Network architectures

For all our baselines, we used the same discriminator and generator architectures, and we controlled the number of latents for a fair comparison. For methods which needs an encoder such as VAEs, VEEGAN, AAE++ and AAE-GAN, the encoder is always set as a convolutional network, formed by transposing the generator (we do not use any activation function after the encoder). All discriminators use leaky units (Maas et al., 2013) with a slope of 0.2, and all generators used ReLUs. In all VAE results, unless otherwise specified, we used a Bernoulli visible distribution and a Gaussian latent posterior.

K.5.1. COLORMNIST

For all our models trained on ColorMNIST, we swept over the latent sizes 10, 50 and 75. Tables 6 and 7 describe the

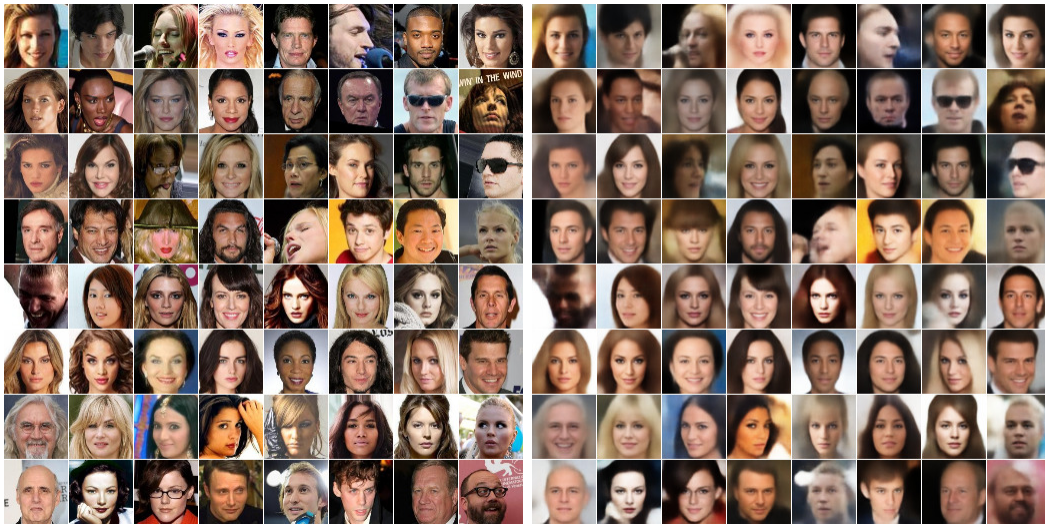
discriminator and generator architectures respectively.

| Operation | Kernel | Strides | Feature maps |
|--------------|--------------|--------------|--------------|
| Convolution | 5×5 | 2×2 | 8 |
| Convolution | 5×5 | 1×1 | 16 |
| Convolution | 5×5 | 2×2 | 32 |
| Convolution | 5×5 | 1×1 | 64 |
| Convolution | 5×5 | 2×2 | 64 |
| Linear adv | — | — | 2 |
| Linear class | — | — | 10 |

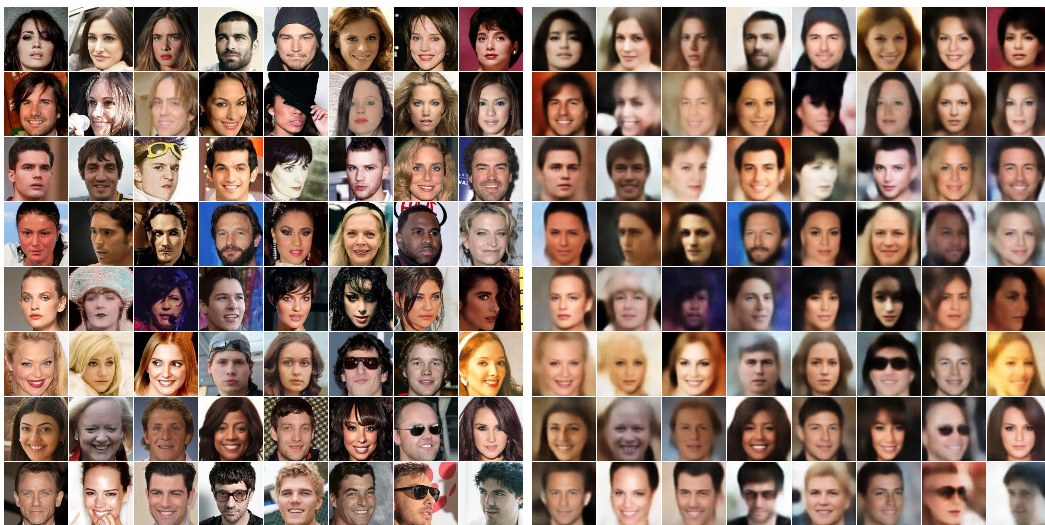
Table 6. ColorMNIST data discriminator architecture used for all models which require one. For DCGAN, we use dropout of 0.8 after the last convolutional layer. No other model uses dropout.

K.5.2. CELEBA AND CIFAR-10

The discriminator and generator architectures used for CelebA and CIFAR-10 were the same as the ones used by Gulrajani et al. (2017) for WGAN, using code



(a) VAE

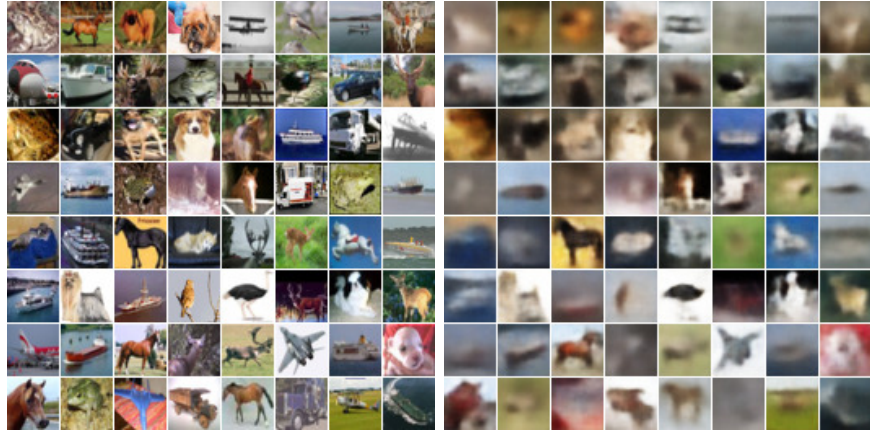


(b) Adversarial Autoencoders

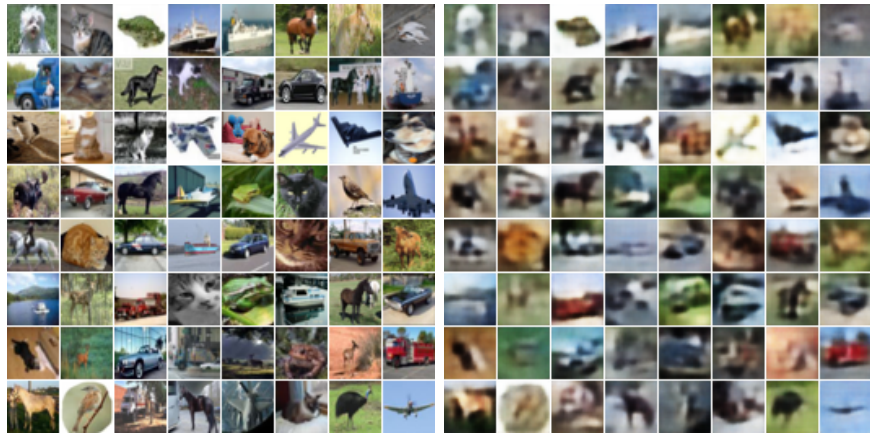


(c) AAE-GAN

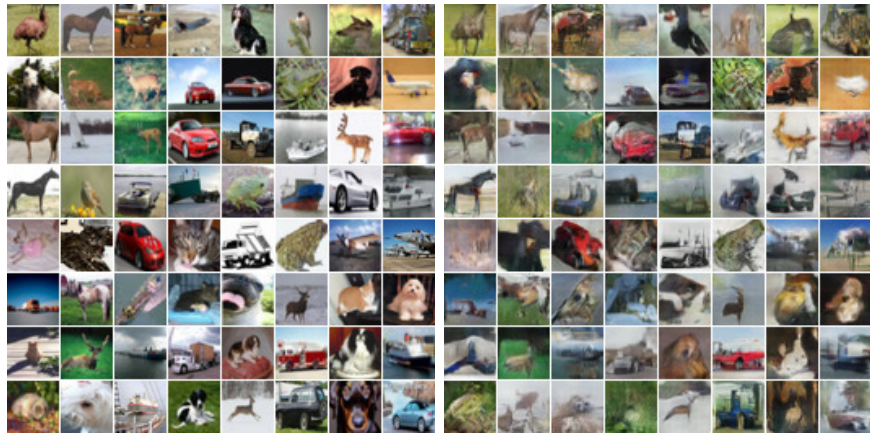
Figure 12. Training reconstructions obtained using a standard VAE, Adversarial Autoencoders and AAE-GAN on CelebA. Left is the data and right are reconstructions.



(a) VAE



(b) Adversarial Autoencoders



(c) AAE-GAN

Figure 13. Training reconstructions obtained using a standard VAE, Adversarial Autoencoders and AAE-GAN on CIFAR-10. Left is the data and right are reconstructions.



Figure 14. CelebA samples.



Figure 15. CIFAR10 samples.



(a) VAE



(b) AAE



(c) DCGAN



(d) WGAN-GP



(e) VEEGAN



(f) AAE-GAN

Figure 16. ColorMNIST samples.

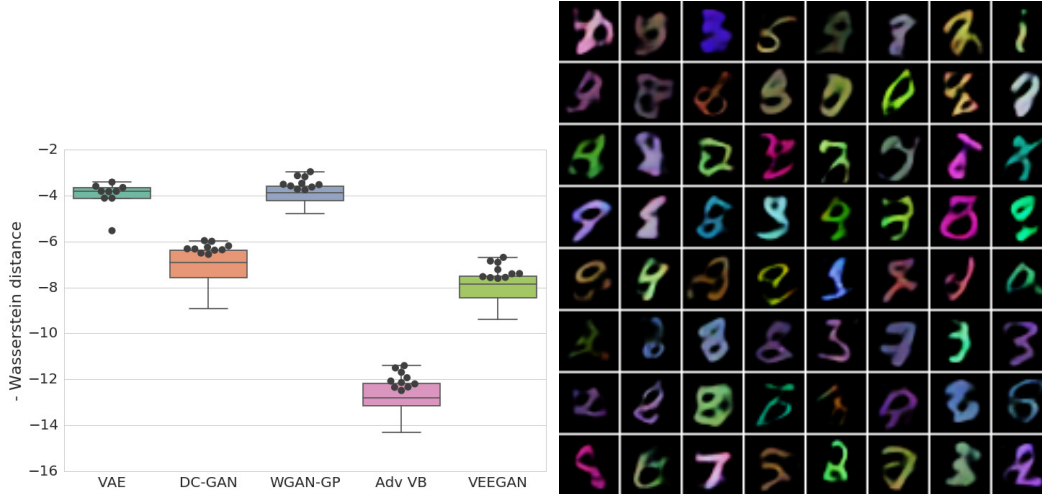


Figure 17. Results obtained using Adversarial VB, without adaptive contrast. The model was not able to match $q_\eta(\mathbf{z})$ and $p(\mathbf{z})$, and this results in an independent critic being able to easily distinguish samples from data (left). This can be seen visually on the right, as the digits do not appear well defined for a large number of samples.

| | Operation | Kernel | Strides | Feature maps |
|------------------------|-----------|--------------|--------------|--------------|
| | Linear | — | — | 3136 |
| Transposed Convolution | | 5×5 | 2×2 | 64 |
| Transposed Convolution | | 5×5 | 1×1 | 32 |
| Transposed Convolution | | 5×5 | 2×2 | 3 |

Table 7. ColorMNIST generator architecture. This architecture was used for all compared models.

at <https://github.com/martinajovsky/WassersteinGAN/blob/master/models/dcgan.py>. Note that the WGAN-GP paper reports Inception Scores computed on a different architecture, using 101-Resnet blocks. For VEEGAN, we designed a code discriminator as defined in Table 8.

| Operation | Kernel | Strides | Feature maps |
|-------------|--------------|--------------|--------------|
| Convolution | 3×3 | 1×1 | [512, 1024] |
| Convolution | 2×2 | 1×1 | [512, 1024] |
| Linear adv | — | — | 2 |

Table 8. The joint discriminator head used for VEEGAN. The input of this network is a vector concatenation of data and code features, each obtained by passing the data and codes through the same discriminator and code architectures used for the other models (excluding the classification layer).

K.5.3. CODE DISCRIMINATOR ARCHITECTURES

For a fair comparison between models, we used the same code discriminator architecture, where one is applicable. We tried both deeper convolutional architectures as well as shallow but bigger linear layers. We found the latter to work best and hence we used a 3 layer MLP with 1000 units each and leaky RELUs activations (Maas et al., 2013) with a slope of 0.2 as the code discriminator. Using 5000 units did not substantially improve results. This can be explained by the fact that too strong gradients from the code discriminator can effect the reconstruction ability of the encoder, and then more careful tuning of loss coefficient is needed. Perhaps optimization algorithms which are better suited for multi loss objective could help this issue.